ELECTRONIC MATERIALS RESEARCH LABORATORY

THE UNIVERSITY OF TEXAS

COLLEGE OF ENGINEERING

AUSTIN

NAS 8-11235

QUARTERLY REPORT

MICROELECTRONICS RESEARCH ON

SILICON-SILICON OXIDE

STRUCTURES AND INTERFACES

February 28, 1965

Submitted to

GEORGE C. MARSHALL SPACE FLIGHT CENTER

NATIONAL AERONAUTICS AND SPACE ADMINISTRATION

by

THE ELECTRONIC MATERIALS RESEARCH LABORATORY
THE UNIVERSITY OF TEXAS
AUSTIN, TEXAS 78712

TABLE OF CONTENTS

Microelectronics Research on
Silicon-Silicon Oxide Structures and Interfaces

LIST OF FIGURES

MICROELECTRONICS RESEARCH ON
SILICON-SILICON OXIDE STRUCTURES AND INTERFACES

i. Theory of M-O-S Structure

The theoretical ratio of minimum capacitance to maximum capacitance and dissipation phenomena are now added to the theory previously presented. This theory resume serves as a guide in understanding the work done in analyzing the experimental results. Most published papers appear to omit certain details needed for a complete reevaluation and comparison of their results. /

A. Theoretical Capacitance Versus Voltage.

The equivalent capacitance is the series equivalent of two capacitors C_o and C_s where C_o is the capacitance of the oxide and C_s is the capacitance of the space charge region of the semiconductor. The oxide capacitance is considered constant and the space charge capacitance a function of the surface potential (in this case the potential of the oxide-silicon interface). The space charge capacitance is given by the following expression:

$$C_s \doteq \beta \frac{\partial Q_{SP}}{\partial Y} = \frac{\epsilon}{L}\left[\frac{\lambda(1-e^{-Y})-\lambda^{-1}(1-e^{+Y})}{[\lambda(Y+e^{-Y}-1)+\lambda^{-1}(-Y+e^{Y}-1)]^{\frac{1}{2}}}\right] \qquad (1)$$

where:

Q_{SP} = the space charge expression developed by Garrett and Brattain.

Y = interface potential in kT units (Figure 1)

λ = normalized doping density to the intrinsic value [$=n_i/n_o = p_o/p_i$]

E = dielectric constant of silicon (1.06×10^{-12} farads/cm)

L = twice the Debye length (4.8×10^{-3} cm)

β = q/kT
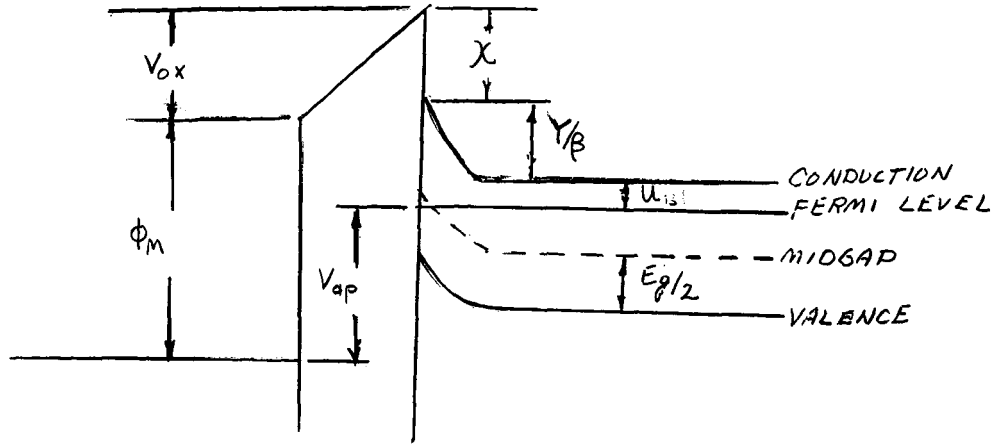
Figure 1

Energy diagram for n-type semiconductor M-O-S
structure which has been biased to inversion.
The arrows give the positive direction of
electron potential.

As long as inversion is negligible $(-Y < \ln \lambda^{-1})$ the equation will reduce

to:

$$C_S = \left(\frac{\epsilon n_0 e \beta}{2}\right)^{1/2} \left[\frac{1-e^{-Y}}{(-Y+e^{Y}-1)^{1/2}}\right] \tag{2}$$

Three special cases of equation (2) are (a) the capacitance of the

accumulation layer

$$C_a = \left(\frac{\epsilon n_0 e \beta}{2}\right)^{1/2} \left[e^{Y/2}\right], \quad Y \gg 1 \tag{3}$$

(b) the capacitance of the depletion layer

$$C_d = \left[\frac{\epsilon n_0 e \beta}{2}(-Y)\right]^{1/2}, \quad 1 \ll -Y \ll 2\ln\lambda^{-1} \tag{4}$$

and (c) the flat band capacitance

$$C_{FB} = \left(\frac{\epsilon n_0 e \beta}{2}\right)^{1/2}, \quad Y = 0 \tag{5}$$

Using these formulas one can calculate the theoretical capacitance

versus voltage curve (Figure 3).

Once the space charge capacitance has been determined the equi-

valent capacitance may be determined using the relation:
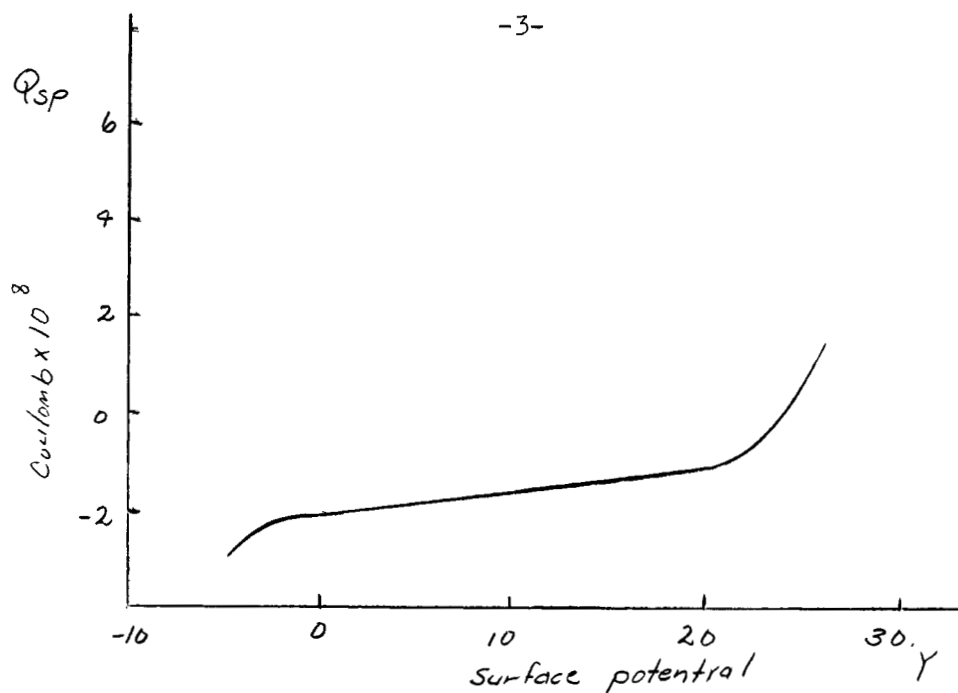
Figure 2

The Theoretical Charge in the Space Charge
Region of n-type 60 ohm-cm Silicon as a Function
of the Surface Potential of the Silicon
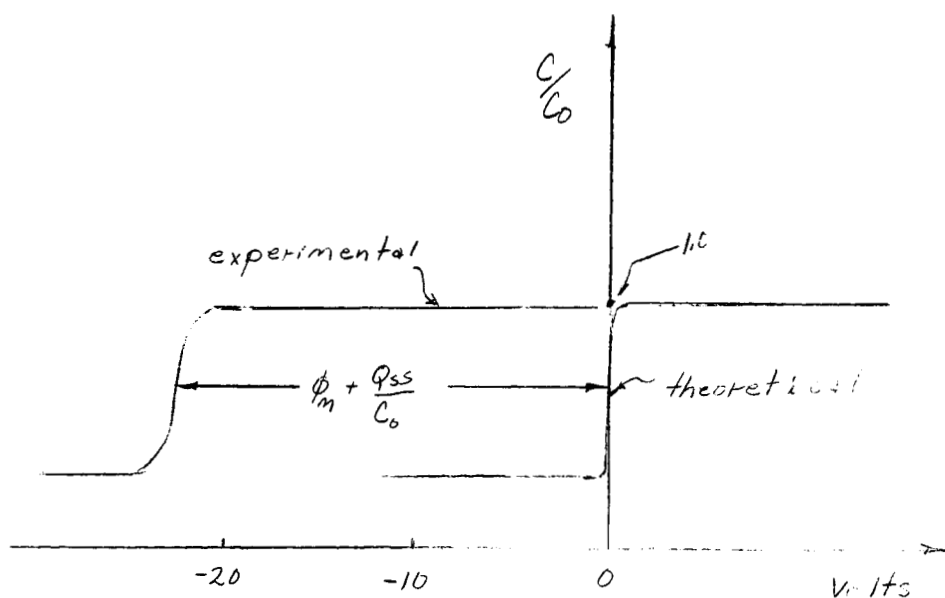
Figure 3

(a) the Theoretical Capacitance vs. Voltage Curve
for 60 ohm-cm n-type Silicon (b) Experimental
Curve Showing the Voltage Shift Corresponding
to Positive Charge in the Surface States.

$$C_{eq} = \frac{C_{ox}\, C_s}{C_{ox}+C_s} \qquad (6)$$

The equivalent capacitance calculated in this manner neglects surface states and if they are present they will show up as a horizontal shift of the capacitance vs voltage curve (Figure 3). The difference in the work functions of the metal and semiconductor will also be present in this horizontal shift but this will be small and can be neglected if the shift is large compared to I volt. The expression for the contact potential can be written down from Figure I using

$$V_{ap} = \phi_m - (\chi + u_B + E_{g/2}) + V_{ox} + Y/\beta \qquad (7)$$

from which the contact potential is

$$V_c = \phi_m - (\chi + u_B + E_{g/2}) \qquad (8)$$

where ϕ_m = work function of the metal

χ = electron affinity for the semiconductor surface

E_g = band gap

B. Approximate formulas for calculating minimum values Capacitance Ratio

The maximum value of the depletion region is assumed to be reached when the concentration in the inversion region is equal to the concentration in the bulk of the semiconductor. Following Grove and Deal this occurs when

$$2\phi_v = q N_D X_d^2 / 2\epsilon \qquad (9)$$

The minimum space charge capacitance at the value of depletion width is

$$C_{s,\,min} = \frac{\epsilon}{X_{d\,max}} = \frac{\epsilon}{L_D}\left(\frac{N_D}{2n_i}\right)^{1/2}[4\ln(N_D/n_i)]^{-1/2} \qquad (10)$$

where

$$L_D = \left[\frac{KT}{q}\,\frac{\epsilon}{2q\,n_i}\right]^{1/2} \qquad (11)$$

and the minimum capacitance ratio is

$$\frac{C_M}{C_o} = \left[1 + \frac{C_o}{C_{s,min}} \right]^{-1} \tag{12}$$

The formula gives some indication of the impurity distribution near the oxide-silicon interface and a more exact formula has been used by Grove and Deal to measure the redistribution of impurities during oxidation of the silicon.

C. Dissipation Phenomena

The initial concept of the contract was to analyze the capacitance data into information about the electronic properties of the silicon/silicon oxide interface. Only recently has significant attention turned to detailed consideration of the dielectric properties of the material. A dielectric constant is associated with any capacitance. Dissipation mechanisms are also inherent in a dielectric material. The dissipation mechanisms appear more closely related to the detailed electronic states and energy exchange mechanisms than does the capacitance.

Qualitatively one can readily see that the M-O-S system must combine the dielectric properties of the glassy oxide layer, the semiconductor surface properties at the interface and the bulk conduction or depletion properties. Each of these has its dissipation mechanisms to contribute to losses in an M-O-S capacitor. This summary of losses in glass covers a topic that has not been accentuated by previous investigations of M-O-S structures.

Dielectric losses generally are the sum of the contributions of four processes: (1) conduction, (2) dipole relaxation, (3) atomic vibration, and (4) network deformation. Figures 4 and 5 illustrate
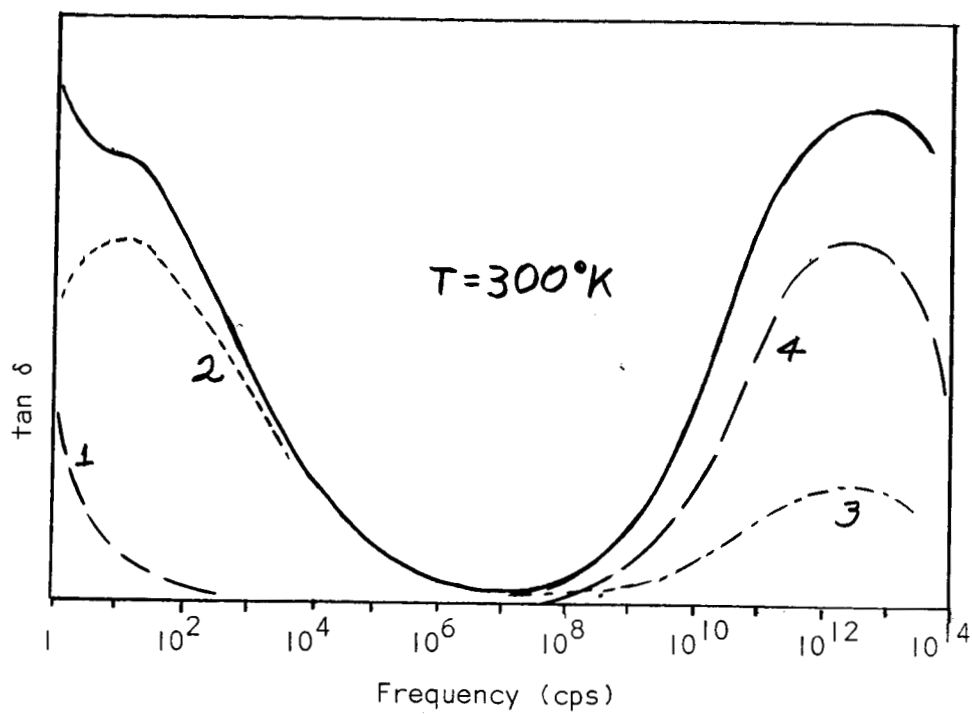
Figure 4

Dielectric Dissipation Losses - 300°K
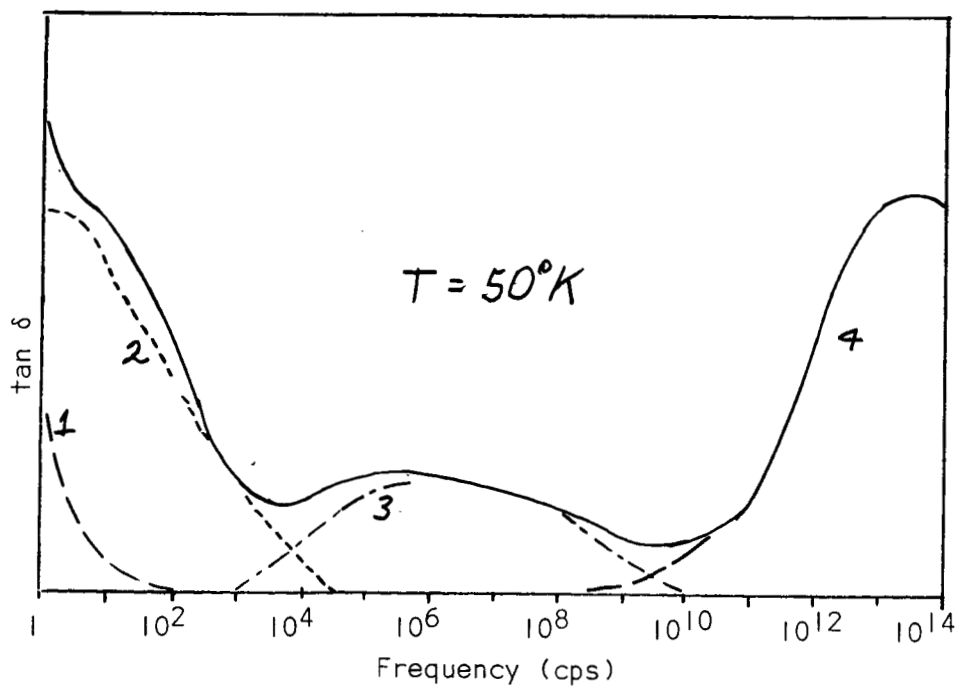
Figure 5

Dielectric Dissipation Losses - 50°K

the relative magnitude of these losses as a function of frequency.

Conduction losses may be identified with the motion of network modifying ions in ordinary glasses. The loss term may be written:

$$\text{Tan } \delta = 1/\omega \rho \epsilon$$

The conduction losses are usually negligible at room temperature above 50 cps. At low frequency and at elevated temperatures, the ionic conduction contributes to the current in the glass dielectric.

The resistivity may be determined by the "rigidity" of the silicon-oxygen network and the properties of other ions added as well as the viscosity, polarization, and diffusion properties of the material. Resistivity of glasses is commonly analyzed in two series type of expressions:

$$\log \rho = \alpha + \beta T + \delta T^2 + \ldots$$

$$\text{and} \qquad \log \rho = A + \frac{B}{T}$$

The second is simpler and can be reasonably well derived from fundamentals through an appropriate model.

The model of an ion jumping from a depression in the curve of potential energy versus position in the network structure to another neighboring depression is the mechanism for both conduction and relaxation losses. The conduction portion occurs because an electric field stimulated drift for a charge ion to allow it to be thermally excited in one direction more easily than the other. The resistivity may be expressed as

$$\rho = \frac{6 \, kT}{\gamma b \eta^2 e^2 n} \, \exp\left(\phi/kT\right)$$

where: T = absolute temperature

ϕ = energy height of barrier to be jumped

γ ≑ frequency of atomic vibration

η = distance the ion jumps (usually from interstice to interstice)

n = concentration of ions under consideration

k = Boltzmann's constant.

b = number of neighboring interstices

e = charge on the ion

This form of equation may be put into the $A + B/T$ form. Experimental measurement of the constant B permits calculation of the activation energy ϕ.

The activation energy ϕ depends on the "rigidity" of the network and the properties of the ion. The rigidity is characterized by the relative number of bridging and non-bridging oxygen atoms in each network polyhedron. Bridging oxygens are chemically bonded to two silicon atoms; non-bridging oxygen bonds to only one silicon atom. As the number of non-bridging atoms increases the structure has more and larger interstices. The structure is then said to be less rigid; atoms may move in the structure more easily.

The constant A depends on the ion concentration, the jump distance for the ion, and the presence of other large atoms in the network. The constant A is inversely proportional to the concentration of ions. The ions cannot move through the network as readily if large ions block the interstitial passages.

Surface conductivity is quite a different thing. It depends strongly on relative humidity and the surface concentration of water soluble ions. Other than these generalities surface conductivity of glasses has received little investigation.

The dipole relaxation losses dominate the conduction losses in most ac measurements near audio frequencies. Ions moving through the structure under electric field forces cause the relaxation losses.

The mean time between transitions is the relaxation time τ. The relaxation time distribution generally follows a Boltzmann factor as in

$$\tau = \tau_0 \, e^{q/kT}$$

where: $\tilde{\tau_0}$ = fundamental period of approximately 10^{-13} sec.

q = height of energy barrier and approximately the same as for the conductivity ion activation energy.

For $\omega \ll \frac{1}{\tau}$ and for $\omega \gg \frac{1}{\tau}$ the dissipation is small. Maximum loss occurs near $\omega\tau = 1$ where the ions move primarily because of the applied electric field. The power factor may be expressed as

$$\text{Tan } \delta = \frac{\epsilon_s - \epsilon_\infty}{\epsilon'} \; \frac{\omega\tau}{1 + \omega^2\tau^2}$$

where ϵ_s = static dielectric constant (dc)

ϵ' = dielectric constant at frequency ω

ϵ_∞ = high frequency dielectric constant

and $\tau = \tau_0 \exp(q/kT)$

The relaxation time has a very wide range of values in a glassy material because of the diverse local structure. Tan δ versus frequency curves exhibit a broad maximum for the relaxation contribution.

Deformation of the silicon-oxygen network constitutes the third loss mechanism. The atomic motion for deformation loss is less than for relaxation loss. This may be visualized as a kind of flexing of the silicon-oxygen atomic chains in the structure; hence the title-- deformation loss. As the temperature decreases, the frequency of maximum deformation loss shifts from high (approximately 10^{10} cps) frequency to medium frequencies (approximately 10^6 cps). The expression for tan δ is the same as for relaxation losses, but the activation energy is less. The deformation losses are usually swamped by the

vibration losses except at 50°K or less.

The vibration losses arise from the damping of the harmonic motion of each atom or radical that can vibrate in the lattice. The resonant frequency is of the form

$$\omega = \left(K/m\right)^{1/2}$$

The multiple masses present and the diverse local structure in a glass means a wide frequency dependence for vibration losses. No sharp distinction exists between vibration losses and relaxation losses.

All the loss mechanisms depend on the chemical composition of the glass. Existing literature discusses high concentrations of lithium, sodium and other ions. Such discussion can be applied only qualitatively to the "high purity" glass on silicon crystals. Generally one can still expect the losses to depend on the nature of the ions, the concentration of the ions, and the rigidity of the network. Water and temperature both influence these considerations strongly.

The literature considered here did not discuss phosphate glasses. The apparent stabilization of planar device oxides by phosphorus makes phosphate glass a prime subject for investigation.

II. Experimentation and Analysis

A. Sample Preparation

The silicon was 60 ohm-cm n-type. The ingot was sliced into discs of approximately 0.030" (30 mils) thickness. The slices were then lapped to a thickness approximately 20 mils and polished in CP-4 to obtain a mirror finish. Thorough cleaning preceded 1200°C wet nitrogen oxidation of the slices.

The lapping process follows

1. Lapping.

a. Lap the 30 mil slice with #240 alumina grit to a thickness of approximately 20 mils to remove the saw damage and to reduce the thickness so that the slice will fit in the quartz boat.

b. Remove the #240 grit by ultra-sonically cleaning in deionized water and lap with #400 grit to remove the evidence of the #240 grit.

c. Again ultra-sonically clean to remove the #400 grit and lap with #600 grit to obtain a smooth surface prior to chemically polishing. Care must be taken in this step so that no scratches appear on the surface because the chemical polish will enlarge them.

d. Ultra-sonically clean the surface prior to polishing.

2. Polishing.

Etching produced a smooth mirror surface. The time for polishing varies from 30 seconds to 1 minute. The reaction is quenched by adding deionized water to the CP-4.

Clean surface preparation is presently an art and not a science. Several methods give satisfactory results. The method used

here follows:

    a. Use deionized water in all cleaning steps.

    b. Clean all glassware and other hardware to be used in the cleaning operation with a suitable non-ionic detergent or cleaning compound.

    c. Scrub the silicon wafers to be cleaned with the detergent.

    d. Place each water in a 50 ml beaker and cover with methyl alcohol.

    e. Ultra-sonically agitate for 30 seconds.

    f. Pour off the methyl alcohol and cover with trichloroethylene.

    g. Carefully heat the trichloroethylene until boiling has been observed for 30 seconds.

    h. Pour off the trichloroethylene and repeat step g.

    i. Pour off the trichloroethylene and flush with water five times.

    j. Fill the beaker half full with concentrated nitric and heat at 80°C for approximately 20 minutes.

    k. Pour off the nitric acid and flush the beaker five times.

    l. Cover the wafer with methyl alcohol for 30 seconds.

    m. Pour off the methyl alcohol and cover with trichloroethylene.

    n. Store in the trichloroethylene until ready to oxidize.

4. Oxidation

    a. Clean the quartz boat and place the cleaned wafers in the boat.

    b. Place the boat in the furnace and oxidize for the desired time at the desired temperature. The slices used in these experiments were oxidized at 1200°C for five hours in an atmosphere of nitrogen and steam.

5. Preparation of the M-O-S Structure

    a. Remove the oxide from one side of the wafer by lapping with #240 grit.

    b. Clean the lapped wafer by ultra-sonically agitating in methyl alcohol for 30 seconds.

    c. Place the wafer in the electroless nickel plating solution and plate the side which has been lapped. A thin film of nickel may plate on the oxide and it should be removed with concentrated nitric acid before depositing the metal contacts.

    d. Place the wafer with an appropriate mask in the vacuum and pump the system to a desired value. A pressure of 1×10^{-6} was used in these tests.

    e. Deposit the gold or aluminum by evaporating it at the proper temperature.

B. Experimental Results

1. Capacitance versus voltage readings were taken at various frequencies over a range of bias values. The frequencies range from 30 cps to 10,000 cps and the bias was varied from -100 volts to +100 volts on a general Radio Type 1615-A Capacitance Bridge.

2. Dissipation factor vs. bias voltage were taken simultaneously.

3. Dissipation factor vs. frequency readings were examined.

4. Leakage current vs. bias voltage was measured using a Tektronics type 575 curve tracer and a Keithley type 610-B Electrometer and Moseley Autograf X-Y recorder.

The curves in Figure 6 represent a typical family of curves obtained by the capacitance vs. voltage measurements. These curves have the same approximate shape as those reported by other workers using similar techniques. The slope of the curve in Figure 6 is greater than that obtained by Kerr. This is possibly due to a difference in
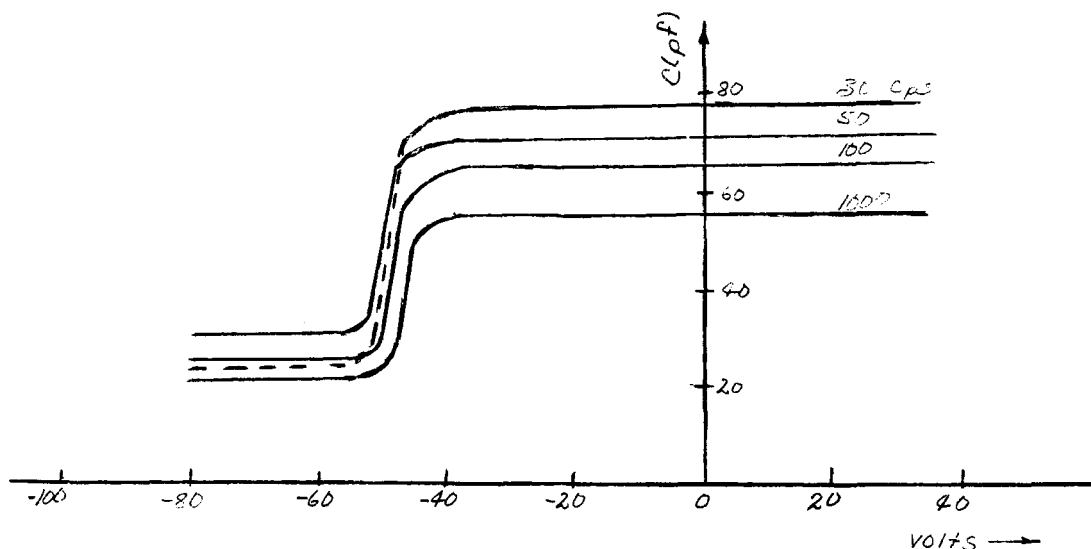
Figure 6

A typical family of curves. The semiconductor used
was 60 ohm-cm N-type with an oxide thickness of
approximately 1 micron. The voltage is that of the
metal relative to the semiconductor.

the manner by which the oxides were grown. Kerr has used a deposition

technique while most of the other workers have grown the oxides by

thermal oxidation. The voltage at which the capacitance started to

decrease varied from -22 to -65 volts on the devices tested. The -22

volts value corresponds to a density of surface states of approximately

2.5×10^{11} cm^{-2} if the difference in work functions of the metal and

semiconductor is neglected. The -65 volts value corresponds to a

density of approximately 7×10^{11}. These values are in close agree-

ment with those reported by Lindner (5×10^{11}) and in order of magni-

tude agreement with values reported by Terman (3.6×10^{12}) and Lehovec

(1.7×10^{12}). Snow, et. al., have observed a shift in this break point

if the device is biased and then heated. They attribute this to a

space charge being created within the oxide. Thomas and Young attri-

bute this space charge to a migration of oxygen vacancies within the

oxide toward the silicon/silicon oxide interface. The devices tested in these experiments were not heated however and tests run several days apart gave results which agree within 1%. The value of capacitance used in these calculations was 1.85×10^{-9} farads/cm^2 which would correspond to an oxide thickness of approximately 1 micron using a dielectric constant of 3.82 for the oxide. The unit area value of capactiance was determined by measuring the oxide capacitance of the device (Figure 3) and dividing by the area of the metal dot. The area of the metal dots used was approximately 1.8 mm^2. Some difficultywas encountered when a larger dot was used in that the oxide would break down under a small bias and short the device. This breaking down of the oxide was attributed to defects in the oxide such as pinholes and thin areas. Breakdown will be discussed later but the oxides were found to fail when the electronic field reached a value of 10^6 volts/cm. Maximum expected value in glass is 10^7 volts/cm.

Deal, et. al, have derived formulas for the ratio of the minimum capacitance to the maximum capacitance based on the impurity distribution in the semiconductor (equation 12). The theoretical value calculated from this equation is 0.45 which compares with values of 0.42, 0.39, 0.42 and 0.385 obtained from the family of curves in Figure 6.

The shift in the capacitance vs. voltage curve corresponds to positive charges in the surface states on all of the devices tested.

Figure 7a shows the dissipation factor associated with the curves of Figure 6. The dissipation factor is defined as 1/Q and in this case is equal to ωRC because the capacitance bridge measures an equivalent resistance and capacitance. The shape of the curves are as would be expected since the dissipation would increase as the capacitance decreases. The considerable
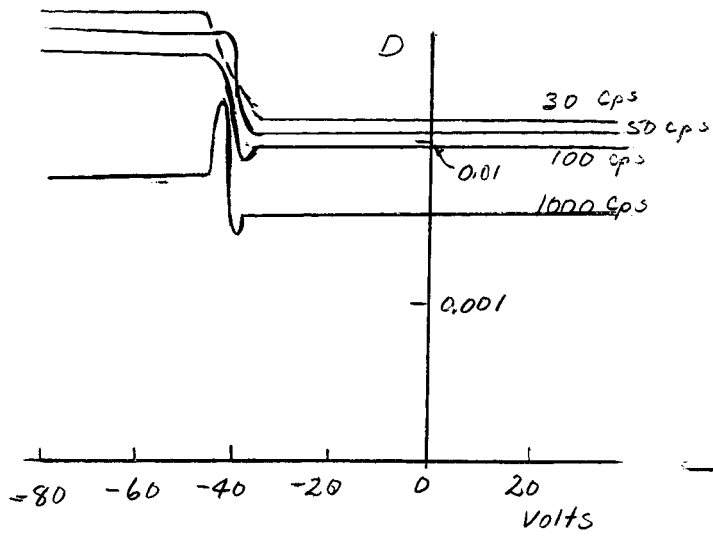
Figure 7a

Dissipation vs. voltage for
the family of curves in Fig.6.
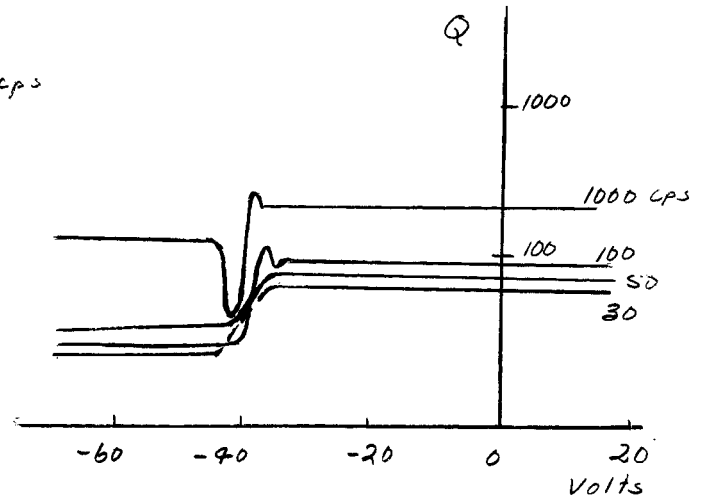
Figure 7b

Quality factor vs. voltage for
the family of curves in Fig.6.

dissipation change with frequency must come from conduction losses. The dipole relaxation loss $D = \omega RC$ permits the dissipation to decrease as the frequency is lowered. However, as Figure 8 shows this is not the case and the dissipation actually increases with decreasing frequency. Dissipation at low frequency offers a potential quality control measurement which could be used easily after appropriate investigation.
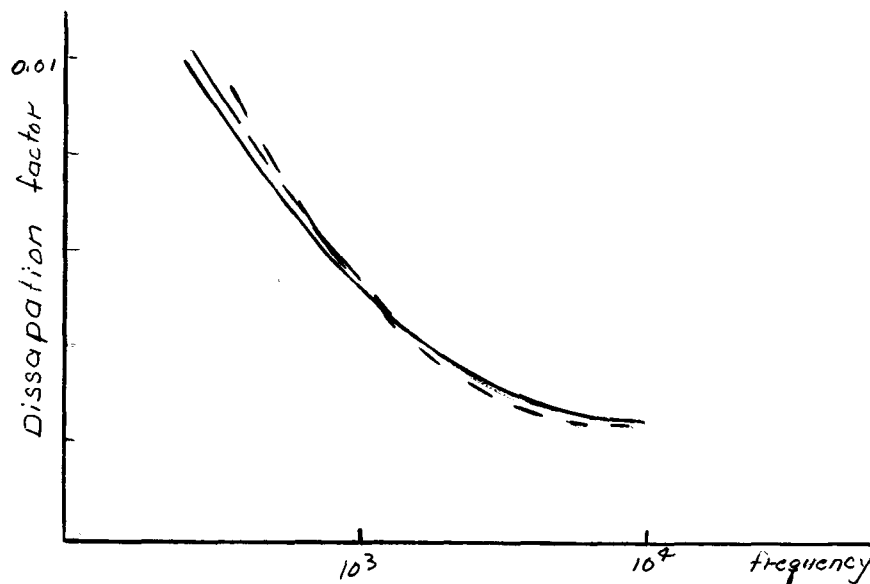
Figure 8

Dissipation Factor vs. Frequency for
a typical Batch of M-O-S Structures.

III. Breakdown Observations

In order to gain a better understanding of the phenomena of break-
down occuring in the M-O-S structures the following tests were conduc-
ted.

A. Breakdown study using the Tetronics Curve Tracer.
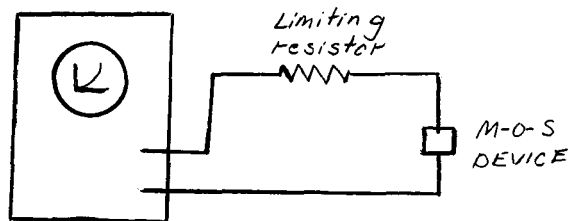
Figure 9

Test Circuit using the Tektronics Curve Tracer
Sweep frequency 120 cps. Maximum vertical
sensitivitiy I microampere per division.

The Tektronics Curve Tracer sweeps a specified voltage range
(from zero to some manually set voltage) at a frequency of 120 cps.
It is possible to change continuously the sweep voltage and observe
the corresponding current-voltage relationship of the oscilloscope.
Figures 10 and 11 show the results of the tests. Figure 10 shows the
structure before breakdown and the evidence of a small current flow.
This seems to indicate that the 120 cps ac impedance is quite different
from the dc impedance. Figure 11 shows the current voltage behavior
after breakdown and clearly the device behaves as a forward diode.

B. Breakdown Study employing Keithley 610-B Electrometer.

The results of this test are shown in Figure 13. The slope
of the leakage current vs. voltage changes sharply from approximately
10^{13} ohms to approximately 10^9 ohms at 6 volts bias. This is not
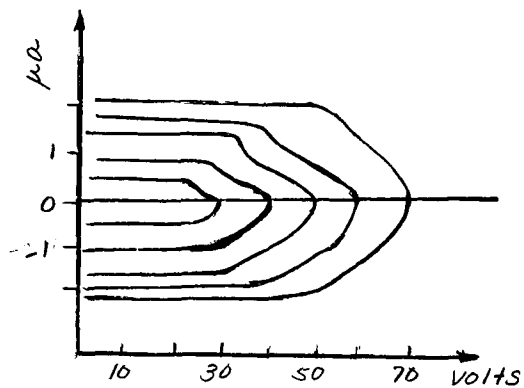
Figure 10

M-O-S I-V Characteristics Before
Breakdown
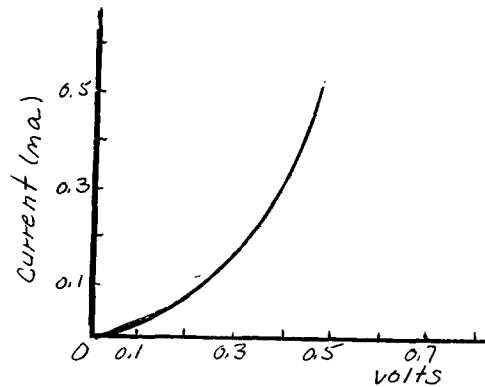
Figure 11

M-O-S I-V Characteristics After
Breakdown

a destructive breakdown because the bias can be reduced to zero and the 10^{13} ohms portion produced again. / The dc resistance after complete breakdown ranged from 10 to 50 kilohms.

These results are preliminary and their explanation is not complete at the present time. They do point to the need to study the breakdown phenomena further and perhaps relate these happenings to changes in the dielectric constant or other parameters. It should be noted that the breakdown was fairly constant on a particular slice but it varied greatly from slice to slice. This could be differences in the surface preparation and handling.
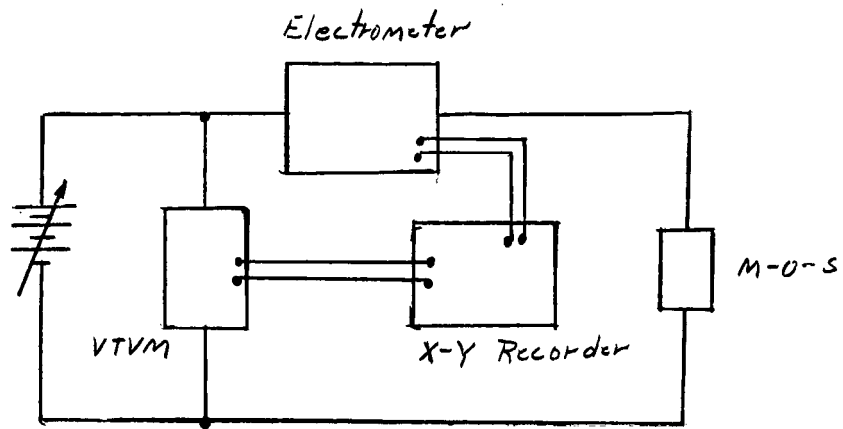
Figure 12

Electrometer Test Circuit
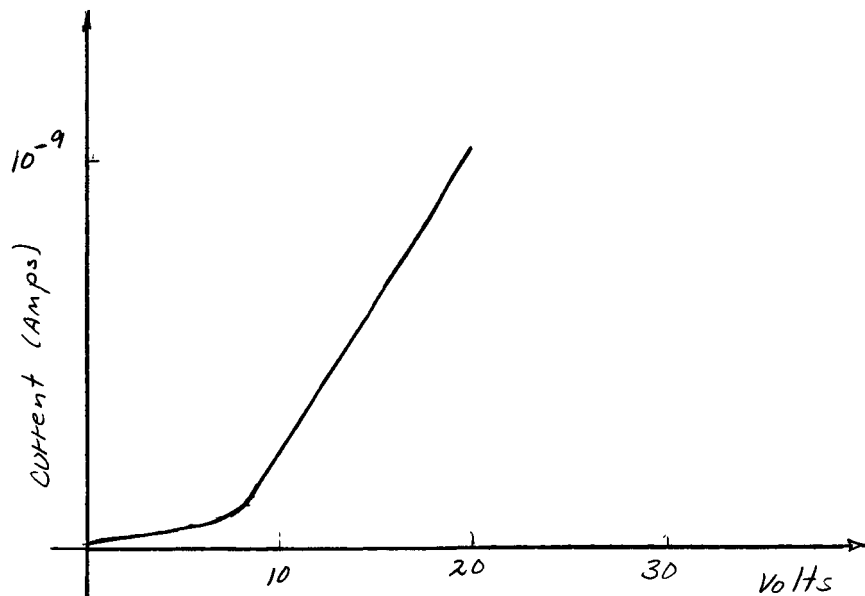
Figure 13

V-I Characteristics Obtained
From Electrometer Test Cirucits

IV . Electron Microscopy

A.   Transmission Electron Microscopy

Activities during this report period have been devoted to improving the sample preparation techniques and observing and studying the samples in the electron microscope.   The procedures required to produce 30 ohm-cm silicon samples have been further developed and it is now possible to obtain about a 20% yield.   The etch process is sensitive because the current must be stopped at just the right moment to obtain a good sample.   About a ten second period defines this point.

Some success has been achieved in etching higher resistivity material. For each resistivity and conductivity type, one must have the optimum current density and jet position.

In order to overcome the difficulty of stopping the current at the correct time, a chemical etch has been employed.   This etch is composed of a 4% (wt./vol.) solution of NaOH to which a 10% NaOCl solution is added until hydrogen ceases to be evolved from the silicon sample.   Best results have been obtained when the solution is maintained between 90 and 100°C.   This etch is very slow acting, requiring up to an hour to etch one micron.   In addition to the slow etching rate, preliminary results indicate that the surfaces prepared by this technique are much cleaner than those prepared by electrolytic etching. However, the surfaces of the samples prepared to date using this technique appear irregular.   This irregularity will not permit the preparation of samples using the chemical etch if an extended period of etching is required.   A combination of electrolytic etching followed by a short period of chemical etching will produce the best results.

Figure 14 is a micrograph of a sample prepared by electrolytic etching until the thin section was less than one micron thick.   Next the sample was
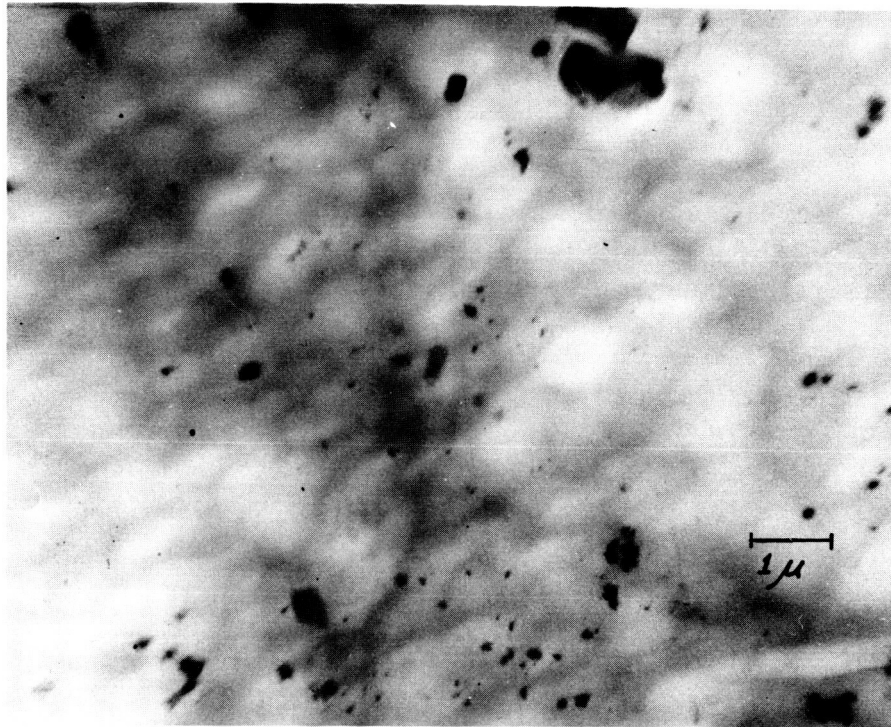
Figure 14
Structure after NaOCl Etch
P-type, 30 ohm-cm Silicon (10,500X)

Figure 15
Striations in Surface Deposits
P-type, 30 ohm-cm Silicon (23,200X)

immersed in the chemical etch for about 30 minutes. The variations in intensity indicate an irregular surface; the dark areas being the thicker portions of the sample. The shape of the light areas does not conform to the expected shape of an etch pit on the [111] plane of silicon. It is therefore felt that the irregular surface is caused by slight variations in etching rates at random points on the crystal surface. The dark masses in the micrograph are due to foreign material which has collected on the sample surface. The shapes of these particles suggest submicron dust particles.

Figures 15 and 16 are transmission micrographs of samples prepared strictly by electrolytic etching. One of the most consistent features in these micrographs is the appearance of very irregularly shaped patches of dense material. It is felt that these patches are a by-product of the electrolyte. The exact cause and composition is being investigated.

Another prominent feature of Figure 15 is the strips of clean and contaminated areas. This phenomena is in all probability caused by variations in the chemical potential of the crystal surface. These variations could be caused by a variety of conditions; two of which are variations in the crystal homogeneity induced during the growing process and variations in impurity types and concentrations which, again, are functions of growth conditions.

The numbered arrows in Figure 16a point out four very similar patterns the nucleus of which are believed to be dislocation loops. The largest nucleus (number 1) is about $700\overset{\circ}{A}$ in diameter. These dislocation loops could have been formed by the collapse of vacancy disks. They are well within the maximum radius of 1.45 microns calculated by Elbaum for the collapsing vacancy disc mechanism. Miller, et al, has published a report on the observance of dislocations formed in this manner and the micrographs presented by him bear a
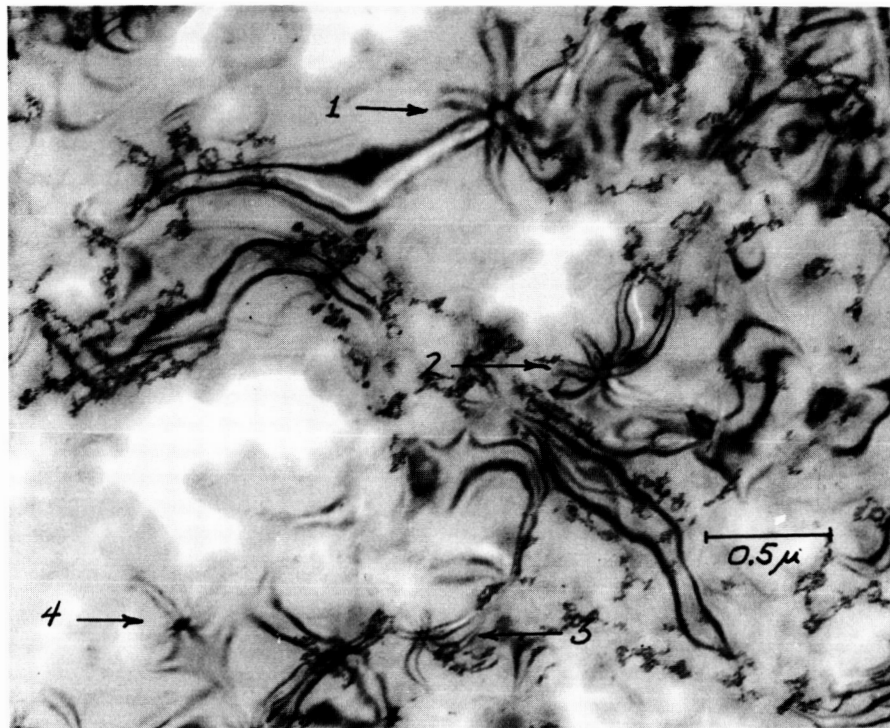
Figure 16a
Dislocation Loops in Silicon-Bright Field
P-type, 30 ohm-cm Silicon (32,000X)
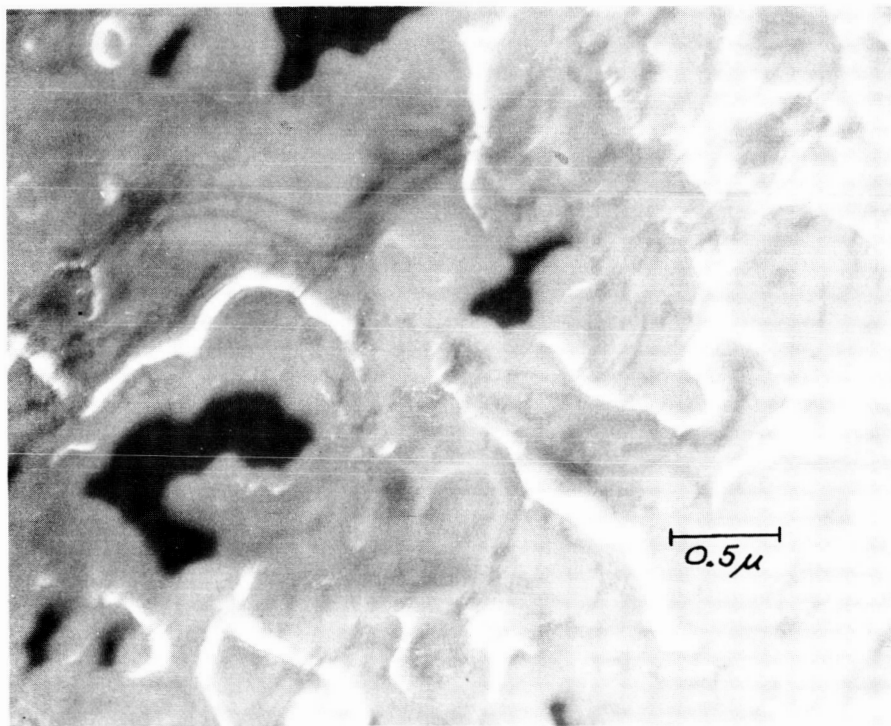
Figure 16b
Dislocation Loops in Silicon-Dark Field
(31,600X)
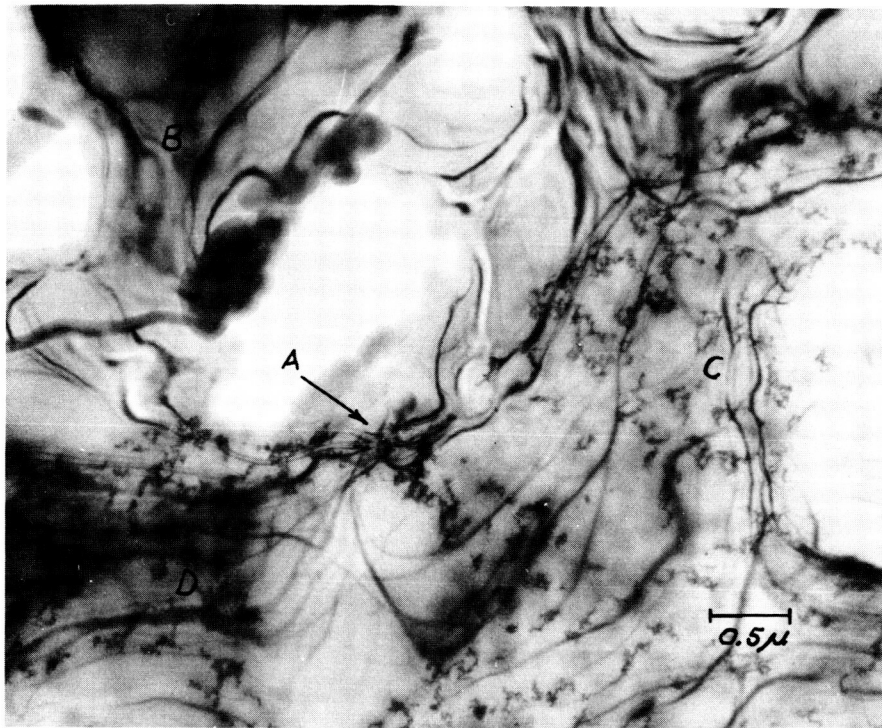
Figure 16c
Dislocation Loops and Extinction Contours
P-type, 30 ohm-cm Silicon (21,200X)

Figure 17
Selected Area [111] Electron Diffraction Pattern
Dislocation Number 1 in Figure 16a

very good resemblance to the loops indicated in this figure. The thickness of
the sample shown in this micrograph is less than 1000A°, therefore the four
dislocations present correspond to an approximate volume density of
$4 \times 10^{12}/cm^3$ or a sheet density of $4 \times 10^7/cm^2$.

The rounded edges of the holes give some information on the etching
process. At the instant that the sample is first penetrated, the material
adjacent to the penetration should be very thin.. However, after penetra-
tion, the electric field strength will increase significantly at the sharp
edge resulting in an increased etching rate at this point. The increased
etching rate will persist until the edges have become rounded and the field
strength reduced to a point comparable to that present in adjacent areas.

Figure 17 is a selected area diffraction pattern of dislocation
Number 1 in Figure 16a. The central ring of Laue spots have the hexagonal
symmetry expected for a beam incidence along the (111) axis of silicon. The
minor spots are due to secondary reflections of the electrons. The light
lines connecting the Laue spots of the inner ring are due to lattice vibra-
tions in the presence of the 100KV electron beam.

Point A in Figure 16C is also a loop dislocation, even though the
nucleus is not as well defined as those in Figure 16a. The apparent appen-
dages to these dislocations are caused by an increase in the strain energy of
the lattice induced by the dislocations. The increased strain energy changes
the diffraction conditions of the lattice. The extinction contour lines of
areas B, C and D in Figure 16C are caused by variations in sample thickness
and differences....They differ in both curvature and density from the lines
radiating from the dislocations. The dark mass in this figure is a sub-
micron dust particle.

Sample preparation techniques are being developed with emphasis on high

resistivity material. Investigation continues on the origin and composition of the observed surface contamination. The filtering stage being added to the electron microscope will improve greatly the ease of specific structure identification in crystalline materials. Replication and transmission examination of the same area will assist in analysis of the surface matter.

B.   Replication of Silicon Surfaces

A new replication method is now used to produce optimum results at this time. This method is a modification of the "collodion" method presented previously.

The new process will be presented in the first section including refinements in the wash method and also the shadowing and evaporation stage. The last section will be a discussion of results which have been obtained including a presentation of several photographs taken in the electron microscope.

New Collodion Method

Methyl ethyl ketone (MEK) is a much better solvent of collodion than amyl acetate. The replication mixture is made in a 10:1 ratio of MEK to collodion.

The replica is made in the following manner: first, one drop of the collodion-MEK mixture is placed on the sample; then a microscope grid is placed in the desired location on the sample in the wet collodion. The collodion mixture will seep up through the grid and will dry holding the grid in place on top of the specimen. After five minutes the collodion is dry and ready to be stripped off. This is accomplished by using scotch tape with a 1/16" diameter hole punched in the center of the tape. After breathing heavily on the sample, the tape is pressed over the sample with the hole centered over the 1/8" diameter grid. It has been found that the moisture from ones breath makes the collodion release from the sample much easier than if this is not done. Immediately after the tape is in place, begin stripping it off slowly, being careful that the collodion does not tear and that the collodion is stripping off the sample. The purpose of the hole in the tape is to prevent as much of the tape as possible from sticking to the sample, thus

preventing contamination of the replica.

At this point the replica is ready for shadowing. As many as ten replicas can be shadowed at once using the following mounting method. Place narrow strips of double sided scotch tape on the two long sides of a microscope slide. Now after the scotch tape - collodion - grid combination is stripped off the sample it is turned over and mounted (sticky side up) across the two strips of tape on the slide. By using narrow tape to strip the grids off the sample, about ten of these can be mounted side by side along the microscope slide.

The correct amount of shadowing is obtained by using about 3/16 to 1/4" of .008" platinum wire wrapped tightly around a tungsten filament (about three turns). For the carbon coating the carbon rods must be sharp and must be held together with a moderate amount of pressure. The vacuum pressure must be less than 4.5×10^{-4} Torr. This system has been able to attain better than 5×10^{-5} Torr. The shadowing angle which has been used is about eight degrees. The replicas have been about 2.5" from the platinum source and about 3.5" from the carbon source. The replicas should be covered first and the electrodes out gased to remove impurities from the carbon, tungsten, and platinum. The replicas are then uncovered and shadowed with platinum then carbon.

The replicas are now ready to be washed. A new wash method has been established which gives a clean replica almost every time. First the grids are removed from the scotch tape by soaking them in ethylene dichloride for a few minutes. After this the grids are place in a jig as described on page 59 of the November 30 Quarterly Report and the vapors of MEK (heated) are passed over the grid for 10-15 minutes. The MEK vapor seems to make the carbon stick to the grid. The MEK bath completes the wash by washing out any remaining

collodion.   The grids are now ready to be examined in the electron microscope.

<center>Results of Replication</center>

The collodion method described above has shown much greater detail than any other method tried, giving resolution of 20Å (based on being able to measure 0.1 mm) before photographic enlargement. Good contrast and intensity is obtained at 50,000X and higher, as shown in the accompanying photographs. Replicas have been made of silicon slices (p-type, 30 ohm-cm) oxided for four hours at 1100°C. Replicas have also been made of p-type, 30-ohm-cm etched silicon samples 1/8" in diameter and about 0.030" thick on the rim, etched to a circular area in the center of less than 500Å thick. Trouble has been encountered with the sample breaking at this thin part when the replica is stripped off. Thus far photographs of replicas have been taken of the same sample which transmission photographs have been taken, but never of the same area because of the problem of the thin area breaking. To make a replica of this structure the above process has been used with the sample mounted on a microscope slide as shown in Figure 18.
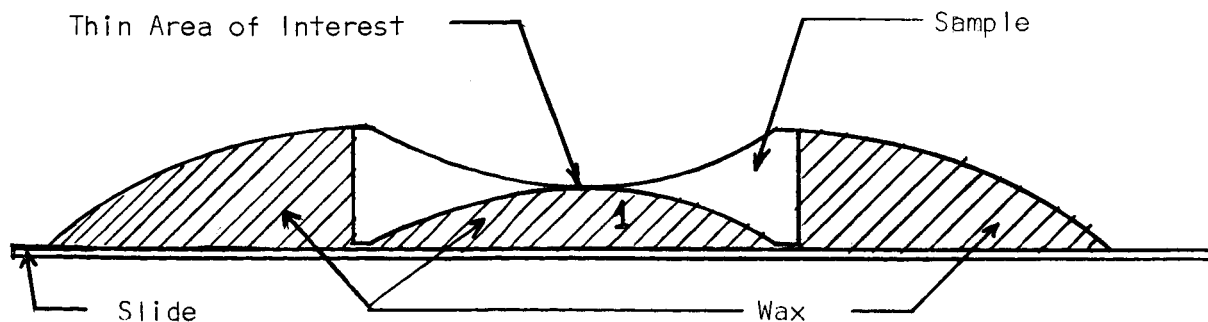
<center>Figure 18
Mounting Etched Silicon Sample</center>

The sample is placed in hot wax so that the wax, when cooled, comes about to the rim of the sample. This minimizes the chances of the replica tearing in the stripping process. It is believed that by getting a better backing of wax or a stronger material in region I in Figure 18 the specimen will not break as easily and replicas will be obtained of the thin area of interest which can then be compared more closely to the transmission micro-scopy photographs. Better results have been obtained from this style sample if the microscope grid is "dimpled" slightly to more closely follow the con-tour of the specimen before it is placed on the sample. In this way the collodion will cling to the grid better and will not tear as easily as if the grid is placed flat across the top. The accompanying micrographs show some interesting features which will now be noted.

One difficulty encountered thus far has been structure observed which might be in the collodion replica. This is shown in Figure 19. Although it is not known at this time exactly what these bubble appearances are, it is suspected that they are in the collodion. Collodion has a tendency to collect moisture and fresh solution should be used to minimize this condition.

The surface structure of the etched silicon can be seen in Figures 20 and 21.which show one sample and Figure 22 which shows another sample. The surface is seen to have a definite texture with small ridges about $500\overset{o}{A}$ apart running across the sample. In these photos the light area with no structure visible is the shadow (absence of platinum). Based on the shadow angle of $8°$ these ridges on the average appear to be $20\overset{o}{A}$ high. Other surface structure does not conform to these dimensions. The sample in Figure 22 appears to have a more irregular texture than that in Figure 21, noting the more varied shadow lengths.

Figures 23 and 24 show respectively an oxide surface and an etched surface for comparison. There is a definite difference in the texture of the two
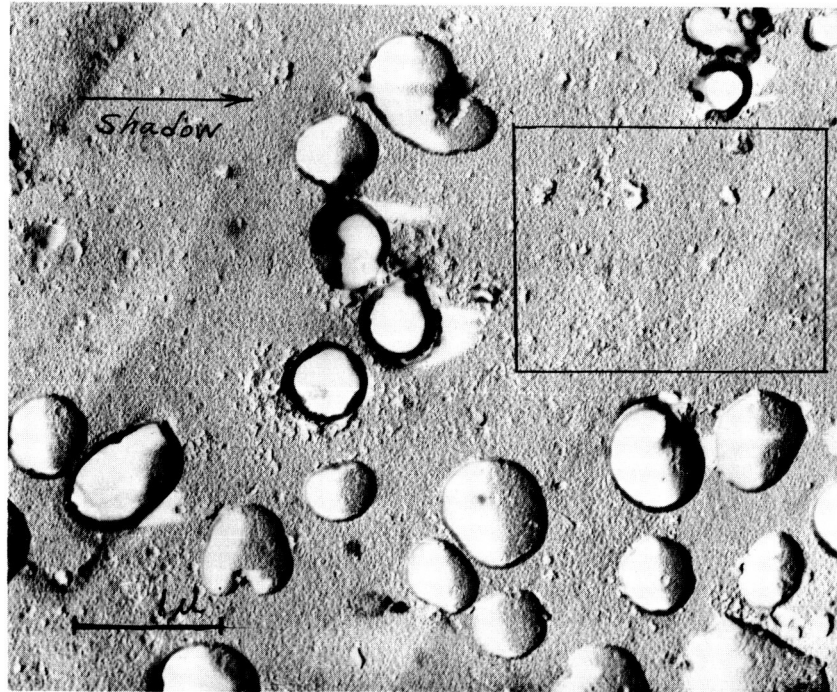
Figure 19
Collodion Properties in Replication
P-type 30 ohm-cm Etched Silicon (19,000X)
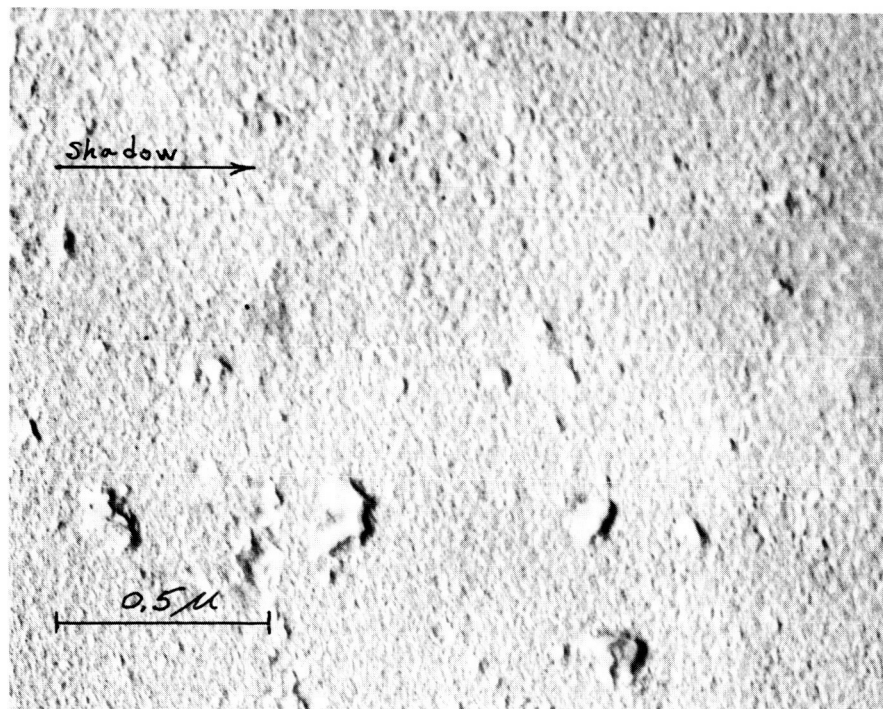
Figure 20
Silicon Surface Structure
P-type 30 ohm-cm Etched Silicon (55,000X)
(Enlargement of boxed area in top figure)

Figure 21
Enlargement of Surface Texture
P-type 30 ohm-cm Silicon (147,000X)
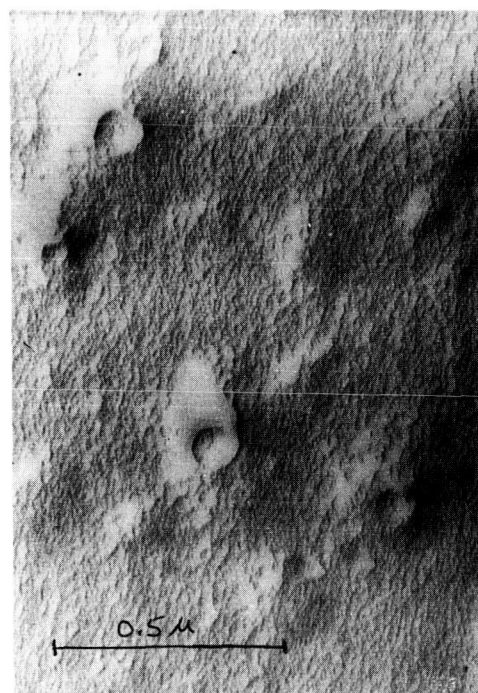
Figure 22
Silicon Surface Texture
P-type 30 ohm-cm Silicon (50,000X)
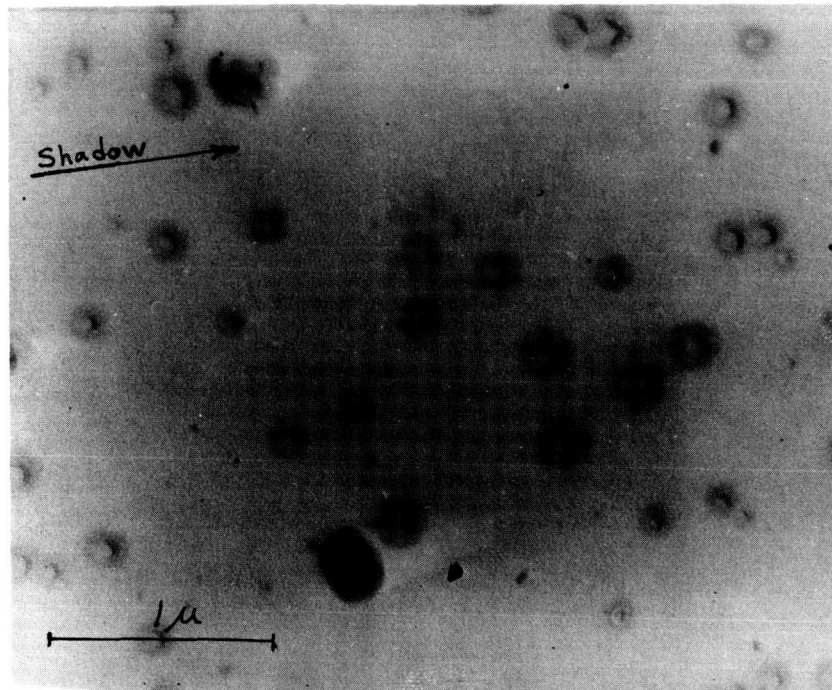
Figure 23
Oxide on P-type 30 ohm-cm Silicon (31,000X)
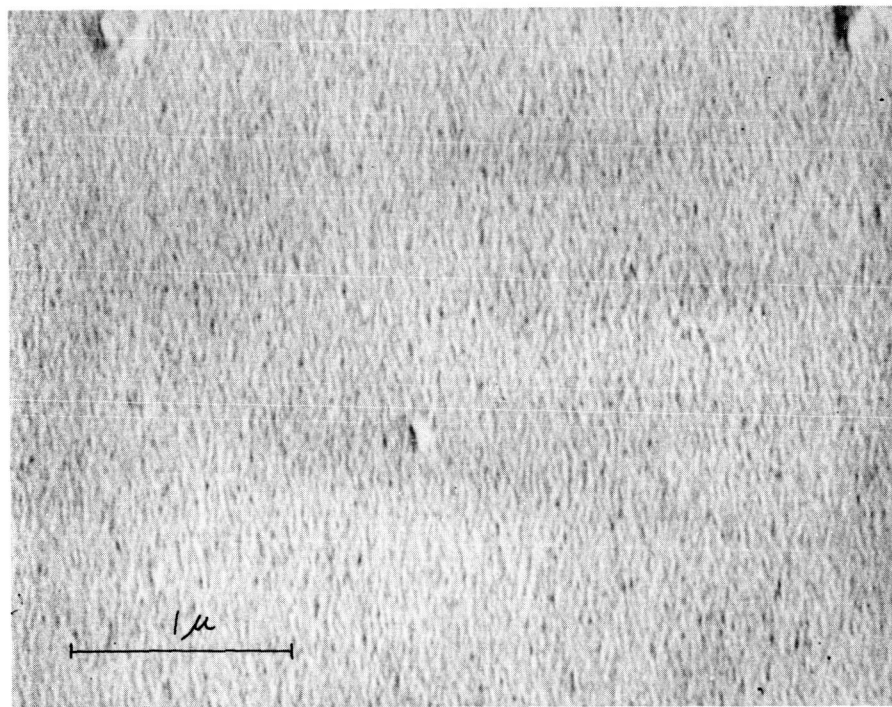
Figure 24
P-type 30 ohm-cm Etched Silicon (29,000X)

surfaces which are at nearly the same magnification. The oxide appears to have a much finer pattern than the etched surface, showing almost no structure. It is not known at this time what the numerous dark places are on the oxide photographs. Several replicas have been made of oxide surfaces all showing patterns similar to this, however, successive exact location replication with shadowing from different directions must be performed before an accurate explanation of these can be given.

In summary, replicas are now being made of flat slices of silicon, oxided silicon, and etched samples in order to complement the capacitance measurements being made. Most of the structural features observed are adequately understood. Replicas of exactly the same area will soon be obtained with which it can be determined whether the structure is on the replica or the surface. Identical area micrographs by both replica and transmission techniques can usually resolve the question of whether observed structure arises from bulk or surface characteristics.

V. Analytical Techniques

The general objective of this research program is an ambitious one. Thorough description for the silicon/silicon oxide system of topography, composition, crystallography, physical properties, optical properties, and electrical properties, will require extensive as well as intensive measurement. Measurement of electrical properties are often strongly influenced by the requirement of having to make electrical contact with the specimen. This section reports further consideration of optical techniques for means of obtaining material parameter information with a minimum number of electrical contacts. Techniques for examining interface carrier-recombination phenomena and surface optical properties by ellipsometry, infrared internal reflection, and luminescence are described.

A. Pulsed Laser System to Study Semiconductors

The solid-state laser, operated in the Q-switched mode, is a unique tool for studying bulk and surface properties of semiconductors. Three properties of the laser beam give it superiority over other light sources; discrete wavelength associated with each of numerous different laser rod materials, abundance of energy in the laser beam, and turn-off times of approximately 20 nanosec.

Bulk and Surface Lifetime Measurement

Of the presently known techniques of semiconductor lifetime measurement, the photoconductive technique and its modifications have found the widest application. In fact, the method has been recommended as a standard by the IRE. However, conventional photoconductive techniques have severe limitations for certain applications. The most serious limitations arise from the light source itself. The absorption coefficient

of semiconductors is large for light in the visible frequencies; as a result, surface recombination often overcomes (or at least interferes with) the bulk recombination lifetime. When filters are used, the light intensity is usually attenuated too much for reliable signals to be obtained from the sample.

Most light pulses are produced by either electronic flashers or chopped light from a "strong" light projector. The electronic flasher, due to large transient currents, often results in interference for the sample signal. The chopped light is usually of low intensity and long delay. Either of these hinderances can be corrected, but only at the expense of the other. A typical decay may last for a few microseconds; the lower limit for measureable lifetimes is therefore fixed at this value.

The conventional solutions to the above problems are:

Filters of the same type semiconductor are placed in front of the sample which allow only the more penetrating (infrared) parts of the radiation to go through, strike, and penetrate the test sample. The measured lifetime is then assumed to be the bulk lifetime. Of course, an undesired effect of the filter is a further attenuation of the already weak excitation radiation. Constant light fills bulk traps. See Figures 25-28.

Surface lifetime is measured by removing the semiconductor filter and using a sufficiently thin sample so that the bulk lifetime is negligible in comparison with the surface recombination.

There is no readily acceptable solution for the long delay of the chopped light. Likewise, there is a practical limit to how intense the light can be made.

The basic change used by EMRL is the utilization of a pulsed laser for the light source. The most significant advantage to the system
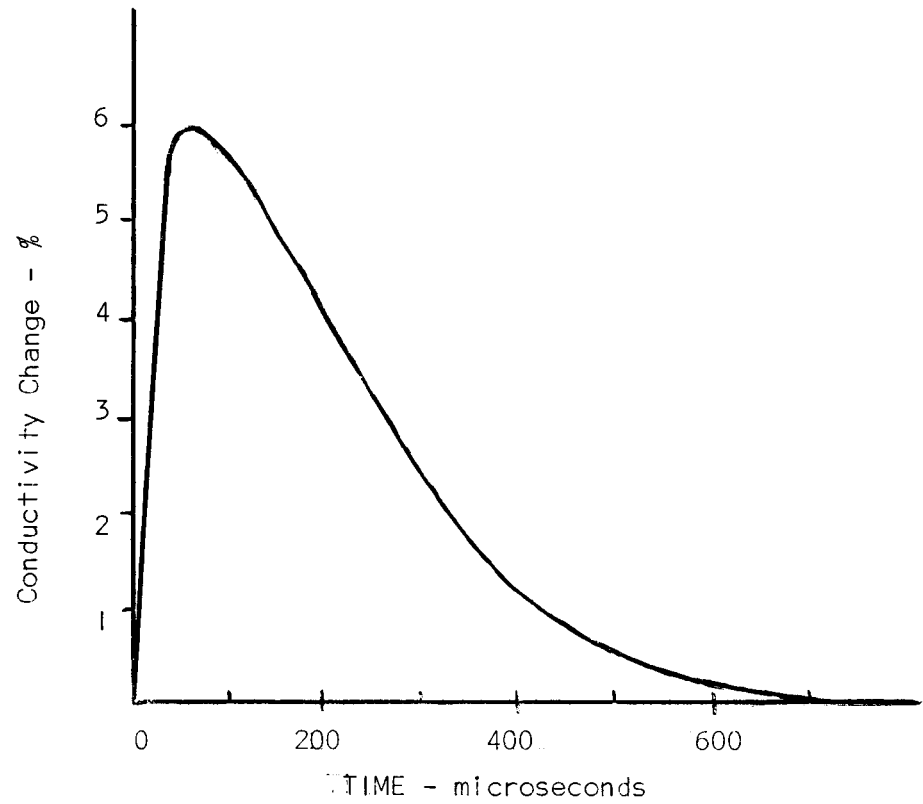
Figure 25
Photo-Conductivity Without Light Filter
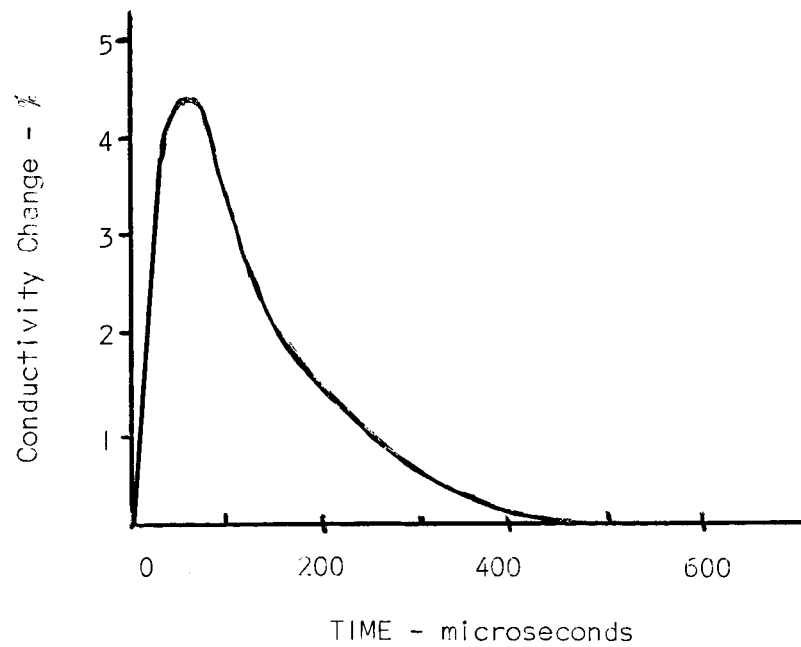
Figure 26
Photo-Conductivity With Light Filter
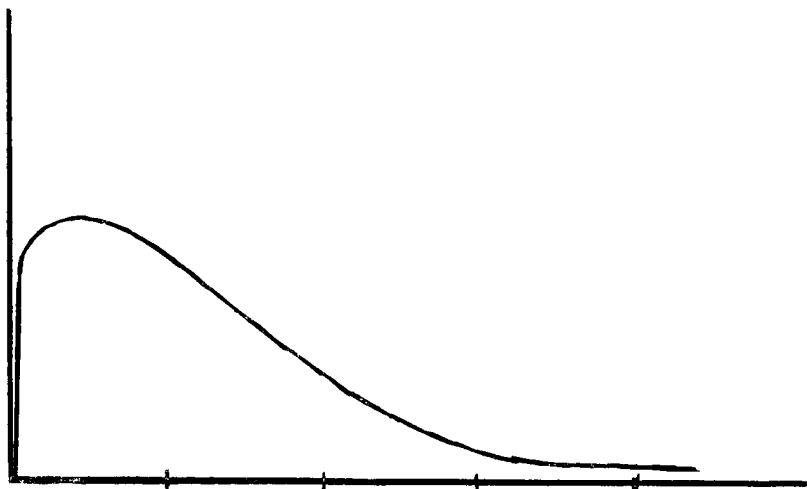
Figure 27
Trap Evidence in Photo-Conductivity
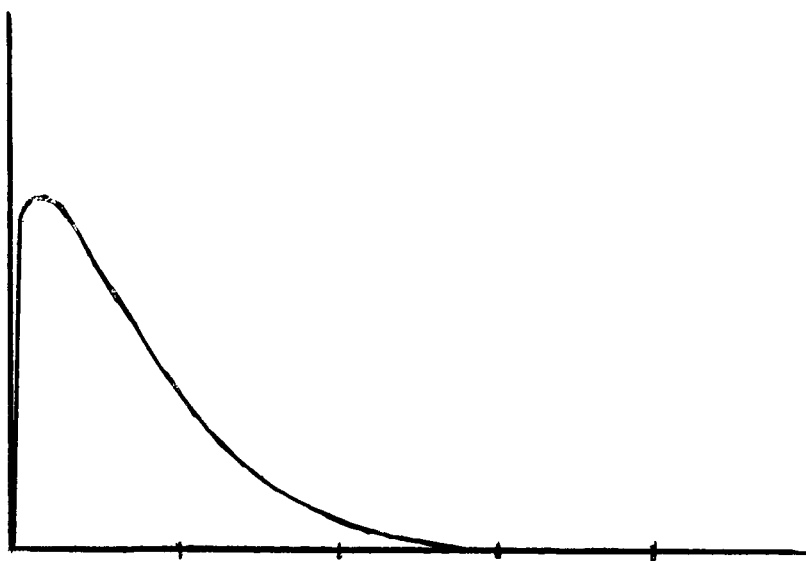
Figure 28
Reduced Trapping by Constant Illumination

is the separation of bulk and surface lifetimes. The choice of laser rods

is sufficiently varied so that rods can be selected whose monochromatic

frequencies enable one to excite the semiconductor both above and below

that corresponding to the intrinsic band gap. Thus one can examine the

surface recombination of samples of arbitrary geometries (thick or thin)

without being concerned with bulk effects by using a laser rod whose

frequency corresponds to a high absorption coefficient of the semi-

conductor. Then by choosing a different rod with a frequency near the ab-

sorption band edge, one can then measure bulk recombination without

using a filter to remove undesired frequency components from the radiation.

Lack of intensity will not be a problem for the EMRL laser.

Filters can be used to attenuate the signal so that the density of radia-

tion produced carriers does not disturb equilibrium conditions.

A Q-spoiled laser, as designed, will be capable of a pulse duration of

less than 100 nanosec., thus the lower limit of measurable lifetimes

has been decreased by more than 10.

The lifetime measurements as of the present time have been made

with the laser xenon flash tube only. The laser rods are now being

installed. This preliminary work has been hampered by the same problems

as are faced by anyone using conventional photoconductive methods. Results

have been most gratifying however. Measurements made on silicon samples

with and without silicon filters have yielded obviously different results.

The conductivity changes when using the filter have proved to be superior

in exponential form (as predicted by theory). The present system produces

unmeasurable (if any) photo-voltage error signal.

Intensity is no problem for the system. Filters are being used to

attenuate the radiation. The xenon light characteristics, as viewed by

an RCA 630 photocell, show light duration to be approximately one milli-second.

The present work, using only the xenon flash tube, was undertaken so as to gain experience with principles of obtaining photoconductive data. Problems of sample biasing, filtering, synchronization of cathode-ray oscilloscope, photographic recording, time and voltage calibration, etc. have been encountered and solved.

Surface Cleaning Study

Several methods have been used to obtain an atomically clean semiconductor surface. An atomically clean surface is by definition one that is free from all but a few percent of a single monolayer of foreign atoms, either adsorbed or substitutionally replacing surface atoms of the parent lattice. In preparation for various measurements of semiconductor properties, a sample is ordinarily cleaned by sand-blasting and polishing or by etching with one of several chemical solutions and rinsing with distilled or deionized water. This type of treatment, while sufficient for most experiments, leaves the surface covered with a film several monolayers thick. The sample will also have large clusters of foreign molecules attached to its surface. However, this is as clean a surface as can be expected at room temperature and atmospheric pressure, since a cleaner surface will adsorb such a film in a small fraction of a second upon exposure to air.

Clean surfaces have previously been obtained by cleavage of a material, growth of a new surface of material, evaporation of surface layer, and by ion bombardment. Ion bombardment is the most common technique for cleaning a surface of an existing material. Resulting surface damage by ion bombardment must be annealed to obtain the basic crystal

structure at the surface of the material. Removal of adsorbed gases and other foreign atoms on a surface is a difficult task.

The exact nature of the adsorption process is not yet fully understood. Semiconductor surfaces adsorb large quantities of oxygen. Heat of adsorption measurements of germanium surfaces suggest that single oxygen atoms are covalently bound to the surface. Hydrogen also appears to adsorb as single atoms. It has been suggested that hydrogen atoms may be buried under the semiconductor surface and not held by covalent bonds. Negligible amounts of molecular nitrogen and carbon monoxide have been observed on germanium surfaces. Several organic gases adsorb on germanium to one monolayer. These molecules appear to be held to the surface by electrostatic forces similar to those of the hydrogen bond.

Even less is known about adsorption on silicon. Oxygen and hydrogen are adsorbed, but experiments disagree as to the type of bonding that is present.

The purpose of this experiment is to determine whether the adsorbed impurities can be released from the semiconductor surface by the energy of light from a pulsed laser. A sample of germanium or silicon is mounted inside a vacuum chamber at a pressure of about 10^{-9} Torr. A pulse of light from the laser is directed toward the sample. Hopefully, the energy from the laser pulse will release the adsorbed materials. The released particles should cause a rise in pressure, which can be observed as an increase in current through the VacIon pump. Since the vacuum pumps are in constant operation, pressure quickly decreases to its original level. Therefore, if the current to the VacIon pump is displayed on an oscilloscope, the resulting trace should show a sharp rise as the laser is fired followed by an exponential decay as the pressure falls back

to the original level. The amount of material removed can be calculated from the pressure and the volume of the chamber.

Dynamics of Q-Switched Lasers

Laser action is light amplification by the stimulated emission of radiation. Some materials such as a few of the rare earth salts exhibit sharp adsorption spectra and fluorescence. By exciting these atoms into a higher energy state by a pumping light, then inducing the emission of light so as to be in phase with a light signal, one has a coherent light amplifier. If a light pulse is reflected through the laser rod several times, its amplitude is greatly increased. Oscillation will occur when the laser gain per unit length, α , which is a function of frequency ν and excess population $n = n_2 - n_1$, exceeds the losses.

Consider a rod of length ℓ between flat, parallel end surfaces L cm. apart. If the reflectivities of these surfaces are R_1 and R_2, then light passing back and forth once between them will be amplified in intensity by $R_1 R_2 e^{2\gamma\ell}$. Define the loss factor γ , here equal to $-1/2: \ln R_1 R_2$, but also including other losses so that the total gain per pass is $e^{\alpha\ell - \gamma}$. Thus, for oscillation at some center frequency, $\alpha\ell = \gamma$. This result is developed more rigorously by Yariv using a resonant cavity approach.

If the losses of the system are kept high at γ_i , while the excess population is increased by the pumping light, then the losses are suddenly reduced to γ , a giant pulse will be produced with energy many times greater than the continuous (CW) laser. Before switching, the excess population inversion is n_i; after switching it tends to n_f, and $n_i > n_f$ for emission. The total light output energy is:

$$U = \frac{1}{2} \hbar \nu \left(n_i - n_f \right)$$

The factor 1/2 appears because the excess population decreases by two for

each photon emitted. For the R_1 transition of pink ruby, $h\nu = 2.8 \times 10^{-19}$ joules, $n_i \sim 0.25N = 4 \times 10^{15}$ at $300^{\circ}K$, and n_f will be between $\frac{N\gamma}{\alpha_0 \ell}$ and zero. Thus, $1/2 \, h\nu \cong 0.56 \, \frac{joules}{cm^3}$, but in practice it is only a small fraction of this due to output coupling, internal losses and non-active crystal periphery. There is a dependence of the giant pulse amplitude and decay on the switching time, which may be broken into two classes, fast switching and slow switching.

Following the work of Hellwarth, Maiman, and Wagner and Lengyel, the time rate of change of photon density, ϕ , and of excess population inversion per unit volume, n, is

$$\frac{d\phi}{dt} = \left(\frac{\alpha\ell}{t_1} - \frac{1}{T} \right) \phi$$

and

$$\frac{dn}{dt} = -\frac{2\alpha\ell}{t_1} \phi$$

where

α = coefficient of amplification = $\frac{\alpha_0 \, n}{N}$

α_0 = adsorption coefficient of laser material

N = number of active ions in laser element $\sim 1.6 \times 10^{19} cm^{-1}$

t_1 = time for single passage of light

T = photon lifetime = $\frac{t_1}{\gamma}$

These non-linear differential equations are valid only for fast switching, i.e., when switching time is so short that ϕ and n are not appreciably altered. This switching time is of the order of 20 nanoseconds and is usually done with electro-optical devices such as Kerr or Pockel cells. By use of some empirical results, the differential equations may be numerically approximated.

Slow switching, in which the inversion population changes during the switching period, is considered by Benson and Mirarchi. Horton extends

the general equations of Hellwarth, as previously presented, to include

slow switching by a rotating reflector and obtains a plot of ϕ and n

versus time. Horton further shows that by proper variation of rod length

and rotation speed to optimum conditions, pulse amplitudes are equal to

those for the fast-switching case. Slow switching has been found to be

less desirable for most applications because of lower power, slower rise,

longer duration, and "after pulses" or multiple pulses.

It has been assumed in the preceeding discussions that the dominant

loss mechanism is the mirror adsorptions. Perfection of reflecting mirrors

is now being accomplished to the extent that this assumption will no longer

be valid, but a satisfactory theory on other losses has yet to be presen-

ted. A study by Menat shows that for power and energy considerations,

the presence of air space or any other media between the ruby and the

mirrors does not appreciably affect the results. The photon decay time,

T, is affected, however, Mace and McCall have shown that shaping the

optical pump pulse shape has little effect on the population inversion,

though it does affect flash tube life.

There are two general types of pulse detection, one a measure of

total energy or power of a pulse, the other a measure of light intensity

versus time, from which power and energy may be calculated.

In early power measurements, the ability of the laser beam to

punch holes in metal foils was used for estimation. This method has

difficulties because the amount of energy feflected and the amount passed

through the hole cannot be accurately determined. Deb et al describe

the black body adsorber in which energy is measured by a rise in tempera-

ture. For energies above about five joules this device is inaccurate due

to incomplete adsorption and deterioration of the material. Higher outputs

can be measured by the deflection of a mirror caused by radiation pressure
on a torsional pendulum.

In measuring the time variation of light intensity, the light
signal is invariably transduced into an electrical or microwave signal.
Brand and collaborators used a germanium block with very short lifetime
to modulate a microwave signal, which was then detected and displayed on
an oscilloscope. Most other methods use photoelectric detectors, such
as phototubes, photoconductors, or photodiodes. There are a number of
commercially available detectors, complete with circuitry. The output
power and energy can be calculated from the oscillograph of the photo-
detector in addition to other information such as rise and fall times,
delay time, and wave shape. Corcoran and Pao have done a study of random
fluctuations of photoelectric detector current on a quantum mechanical
basis. Their work shows that for high-intensity radiation, such as with
a laser, the photon noise dominates rather than shot noise, although
shot noise dominates for ordinary light experiments. Forrester, Gudmund-
sen and Johnson and Brown and Twiss have proved this experimentally.

Pulsed Laser System

A Q-Switched Pulse Laser System is used for semiconductor research
in the Electronic Materials Research Laboratory. The major components in
the system are the power supply, the synchronizing circuit, the laser head
and its trigger circuitry, the optical bench, the Porro-prism Q-Switch,
and the associated equipment. Figure 29 illustrates the arrangements of
the components.

The synchronizing and trigger circuit incorporates a phase shifter
circuit to make small changes in the input signal with respect to the posi-
tion of the Q-Switch prism, a pulse generator driven by the input signal,

and a thyratron trigger to initiate the firing of the pump lamp. Outputs
are provided for monitoring all portions of the signal throughout the
circuit with trigger outputs for oscilloscope external triggering.
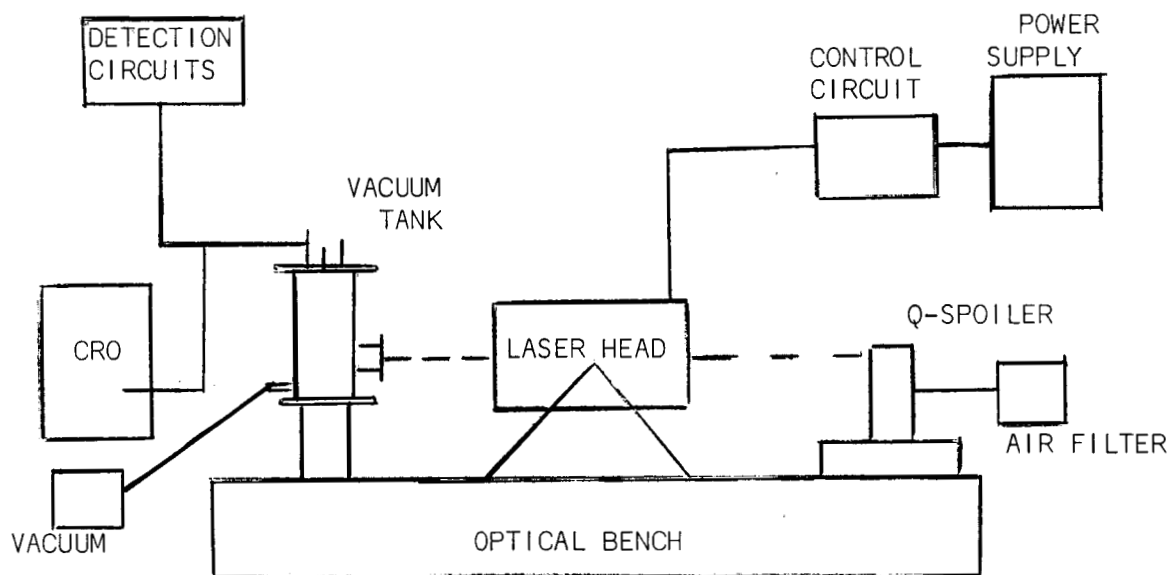
Figure 29
Block Diagram of Pulsed Laser Apparatus

The laser head with its related wiring consists of a cylindrical
container with ceramic chuck for mounting the laser rod, a trigger capacitor
and transformer, helical xenon lamp, and two power leads, one for trigger-
ing, and the other for the high voltage pulse from the power supply. A
blower provides forced convection cooling for the lamp. Some modifica-
tions were made to adapt the head for mounting on the optical bench.

The Q-Switch was manufactured by the Beckman-Whitley Company. It
consists of an air-turbine as the prime mover for the Porro prism. The
rotational speed is continuously variable up to 1500 rps. The prism can
accomodate a laser beam up to 1/2" in diameter. Filtration prevents

foreign matter from entering the mechanism, since small particles of dust in the bearings will cause rapid wear. Particles of dust or a film on the prism face can cause scattering of the laser beam. A two-stage air filter system for the Q-Switch has been constructed to minimize particulate contamination.

The first filter stage consists of a cylindrical tank with several baffles through which the air flows. The spaces are filled with coarse f filtering material consisting of mats of rubberized horsehair. This stage removes large particles such as pipe caulking or dirt. . The second stage will consist of another cylindrical tank containing a dry=type air filter element as used for an automobile. This stage will remove very small particles which may penetrate the first stage. Other filtration techniques may also be useful.

Part of the associated equipment includes an evacuated container for the semiconductor sample. This container is mounted on one end of the optical bench, and has a window through which the laser beam can pass. The top is bolted down over an O-ring during operation when the container is to be evacuated. Feed-through connectors are provided for the internal circuitry. Provisions for controlling the temperature of the sample through a coolant cavity and heater coils are included. At present, pumping down with a mechanical pump can be accomplished to avoid heat loss by convection between the sample and the sides of the container. In the future, a similar container will be constructed of stainless steel with standard vacuum fittings to be used with sorption pumps and an ion pump for a very high vacuum. High vacua are needed for studies of adsorbed gas removal from semi-conductors, discussed below.

Controls and metering facilities are located on the panel to

provide the proper biasing of the sample. A power supply used as a current generator with several ranges of biasing resistors, heater controls, and oscilloscope monitoring with photography capabilities are included. Also a trap light is directed onto the sample to fill traps in the semiconductor before firing the laser.

The present capabilities of the system are summarized here in tabular form.

Power Supply and Helical Flashlamp

Max. Input energy 3000 joules at 5KV

Pumping pulse 1.5 ms

Energy output 6943A, 10600Å at   1 joule

Flashlamp life   10,000 flashes depending upon pumping level.

Flashlamp voltage threshold   3000 volts

Mode of operation: Manual charging, preset limit variable 0 - 5000 volts

Total storage capacitance 240μf in increments of 40μf

Triggering method: Thyratron switch tripped by pulse in synchronization
                    with external signal such as Q-Switch

Safety precautions: all cabinet doors interlocked with capacitor discharge
                     circuitry, also all capacitors shunted in event of
                     power failure.

Optical System

Laser Head: 1/4" x 2" rods in silvered cylindrical cavity

Rods: Al_2O_3, .05% Cr_2O_3 [One TIR rod, One BEF rod]
      $BaWO_4$, .04% Nd^{+++} One BEF rod

Output pulses: either normal or Q-Switched mode

Cooling: provision for air cooling into laser head, either ambient temper-
          tures or precooled air.

Q-Switch: Rotating porro prism, maximum beam diameter, 5/8", maximum

        speed 1500 rps

Minimum pulse duration: 50 nanoseconds at maximum rotational speed

5 volt synchronizing output

Optical bench: 1.5 meter linear optical bench with Q-Switch carriage

        capable of horizontal adjustments accurate to $\pm$ 10^{-4} inch

        and tilt adjustments accurate to $\pm$ 1 seconds of arc. Manual

        coarse adjustment of distances between components, i.e.,

        sample holder, laser head, Q=Switch.

B. Ellipsometry

If a light beam is directed onto the sample, part of it may
be reflected and part of it may pass through. If the light beam is
monochromatic and polarized, it suffers attenuation and phase shift
on either reflection from or transmission through the sample. This
leads to two methods of measuring film properties, i.e. by measuring
and comparing the properties of the reflected or transmitted light to
those of the incident light. Changes in relative amplitude and phase
of polarized light are dependent on the conductivity, the thickness,
the dielectric constant, and the angle of incidence to the sample.

For a variety of samples of varying thickness, reflection meas-
urements are best. Transmission can be used only when the thickness
is such that a measurable amount of light passes through the sample.
Reflection measurements can be made at normal incidence to the sample
or at some angle, but certain measurement difficulties occur at
normal incidence. It is best to direct incident light at some angle
to the surface.

The detailed theory involved in feflection is well explained
elsewhere, so only the important results will be included at this
point. Fig. 30 shows a substrate and one film. Plane polarized, mono-
chromatic light is incident at an angle ϕ_0 with a normal to the surface.
It is partly reflected from the surface of the film. Some light is
transmitted on through the film and reflected at the film-substrate
boundary. These two reflections combine to form the reflected beam.

For reflection at a boundary, Snell's laws are applicable and
we have :

$$\text{Sin } \phi_0 = \text{Sin } \phi_1$$
$$N_1 \sin \phi_0 = N_2 \sin \phi_2$$
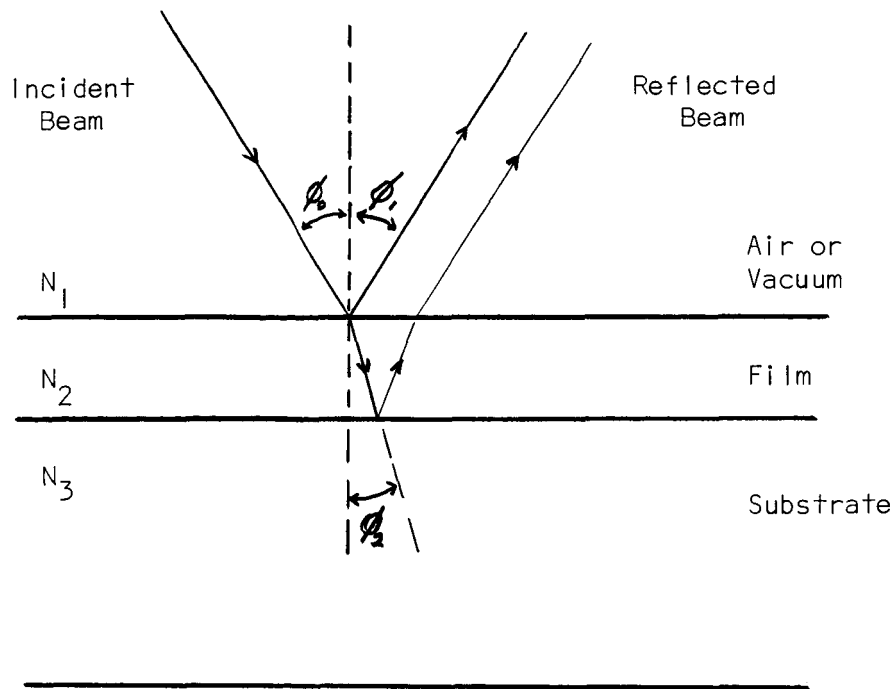
Figure 30
Light Incident on Single Film Layer

where N_1 and N_2 are the indices of refraction. For conduction materials, a complex index of refraction must be defined, $N = n + jk$. J. Stratton's Electromagnetic Theory gives a good treatment of complex indices of refraction. The quantities n and k are related to conductivity by

$$\left(n + j k\right)^2 = \omega^2 \epsilon \mu + j \omega \sigma \mu$$

By resolving the incident wave into s and p components (perpendicular and parallel to the plane of incidence), and using Maxwell's equations, it is found that these components are not changed by equal amounts on reflection. Reflections are described by a reflection coefficient r, and phase shift δ , which are ratios of amplitudes of incident to reflected light and phase changes on reflection.

$$r_p = \frac{N_2 \cos\phi_0 - N_1 \cos\phi_2}{N_2 \cos\phi_0 + N_1 \cos\phi_2}$$

$$r_s = \frac{N_2 \cos\phi_2 - N_1 \cos\phi_0}{N_2 \cos\phi_2 + N_1 \cos\phi_0}$$

When the reflections from the film-substrate interface are included, the

following relation for total reflection and phase shift results.

$$\rho e^{j\Delta} = \frac{Y_{1p} + Y_{2p}\, e^{-2j\delta_1}}{1 + Y_{1p}\, Y_{2p}\, e^{-2j\delta_1}} \times \frac{1 + Y_{1s}\, Y_{2s}\, e^{-2j\delta_1}}{Y_{1s} + Y_{2s}\, e^{-2j\delta_1}}$$

$$\delta_1 = (360/\lambda)\, t\, (N_1^{\,2} - \sin^2\phi_0)^{1/2}$$

Reflection at the film surface is denoted by r_{1p}, the subscript p denoting

the p polarized wave. Reflection at the film-substrate interface is

denoted by r_{2p}. The ellipsometer measures ρ and Δ.

    Consider an end view of elliptically polarized light as shown in

Fig. 31. There the ellipticity is described by the angles χ and α.
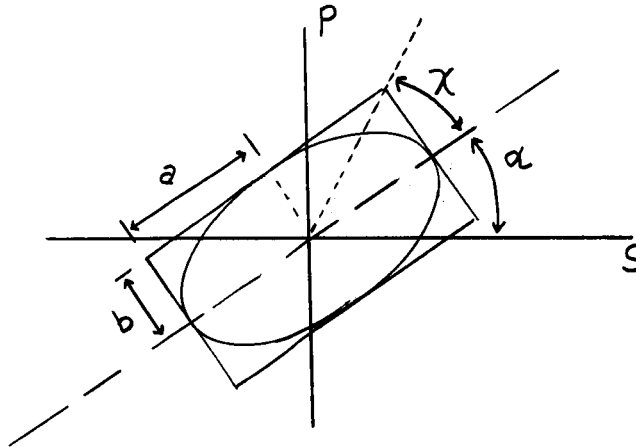

Figure 31
Nomenclature for Elliptically Polarized Light

From these and trigonometric identities, it follows:

$$\text{Tan } 2\chi = \text{Tan } 2\psi \cos \Delta$$

$$\text{Sin } 2\alpha = \text{Sin } 2\psi \sin \Delta$$

$$\text{Tan } \psi = \rho$$

Thus, by working back from ellipsometer measurements, a value for dielec-

tric constant conductivity and thickness may be found.

In practice, finding a value for these parameters is not so simple
as desirable. First, one set of ellipsometer readings may correspond to
several different film situations. Therefore, several readings must be
made and curve fitting techniques employed.

The second problem involving the technique is that the equations
to be solved are very complex. With conducting films, complex indices
of refraction and complex angles occur. Therefore, governing equations
must be solved by some approximate method such as Drude's approximation
or by use of a computor to solve the exact equations. Computor programs
for this purpose have been written and one should be available soon.

Ellipsometer measurements can be very accurate with good equip-
ment and careful laboratory work. The complex index of refraction can be
measured to three significant figures and thickness to $\pm 1 \overset{\circ}{A}$. Obtainable
accuracy varies somewhat over the thickness ranges with more difficulty
in measuring very thin films. Dielectric constant and conductivity values
are less accurate but should be as good as or better than other methods.

Detailed consideration of ellipsometry reveals that the use of
multiple angles of incidence and polarization can give several simultane-
ous equations soluable for dielectric constant, (ϵ), magnetic susceptibi-
lity (μ), and conductivity (σ), we well as the thickness. Thorough
discussion of ellipsometry can be found by F. L. McCrackin, et al, Journal
of Research, A. Vol. 67A, No. 4, August, 1963, pages 363-377 and by
K. H. Zaininger and A. G. Revesz, RCA Review, Vol. 25, No I, March, 1964,
pages 85-III.

Figure 32 presents the essential elements of an ellipsometer. Ellipsom-
eters of high quality may be purchased from O. C. Rudolph & Sons, Co. and
Gaertner Scientific. Karl Lambrecht Optics Company can supply precision

special optic elements. General opinion found among scientists using ellip-
sometry is that Gaertner's is the best make of instrument commercially
available.

Figure 31
Ellipsometer

LEGEND
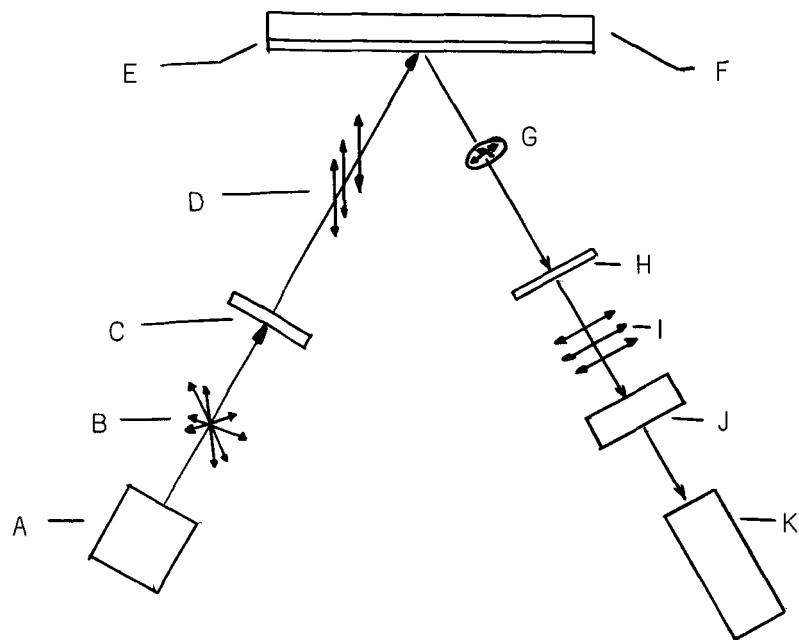
A.   Light Source

B.   Nonpolarized Light

C.   Nicol Prism

D.   Plane-Polarized Light

E.   Thin Film

F.   Substrate

G.   Elliptically Polarized
     Light

H.   Quarter-Wave Plate

I.   Plane-Polarized Light

J.   Analyzer

K.   Detector

C.   Infrared Internal Reflection

Every molecule has associated with it certain energy levels. These levels may correspond to allowed transitions of electrons within each atom, the binding energies associated with the chemical bonds, vibrations caused by thermal agitation of these bonds, or translation and rotation of the molecule itself. In theory, if all the discrete energy levels of a molecule are known, then the molecule can be identified. If a molecule is radiated by an electromagnetic wave oscillating at a frequency f (corresponding to an energy E= hf), the energy can either be reflected, absorbed, or partially absorbed. Absorption takes place when the energy of the incident wave corresponds to a particular energy level within the molecule. Reflection takes place when this condition is not met. In some instances the incident wave may be greater than the required energy associated with the molecule, in which case some of the wave may may be absorbed and some re-radiated at a new frequency corresponding to the difference of the initial and absorbed energy.

If a spectrum of frequencies is passed through a substance, a plot may be made of the percent of the incident radiation absorbed versus the wavelength of the incident ray. This plot is called the "absorption spectrum" of the substance in question. The type of spectroscopy involved depends upon the frequency of the electromagnetic radiation involved.

Classical electrodynamics shows that interaction between waves and molecules in the form of emission or absorption is only possible if the interaction is connected with an alteration in the electrical dipole moment of the interacting molecules. The same result is obtained by application of quantum theory. Only those rotations and vibrations which cause an alteration in the electric dipole moment are excited by radiation, i.e. can be measured by absorption methods. These are generally called

infrared active. Nothing can be learned from the infrared absorption

spectrum about rotations and vibrations which do not cause alterations

in the dipole moment. In order to investigate these, it is necessary to

use another phenomenon, the molecular scattering of electromagnetic waves

known as the Raman effect.

In general, one obtains absorption of energy only if the incident

photons possess precisely the correct amount of energy for the transition

to take place in the atom or molecule. Raman spectroscopy is based upon

an exception to this rule, for frequencies in the visible or ultraviolet

regions may, under certain circumstances, be partially absorbed, causing

the molecule to vibrate or rotate. The photon is re-emitted with a new

frequency, less than the original, as required for conservation of energy.

The frequency of the Raman line, f_r is given by the equation

$$f_r = f_E - f_V$$

where f_E is the frequency of the incident radiation and f_V is the vibra-

tional frequency of the molecule. The probability for this partial absorp-

tion is quite small.

The infrared spectrum is divided into three sections: near, inter-

mediate or middle, and far infrared regions. Most of the work in molec-

ular vibrations is done in the middle region, although some research has

been done in the near region. Molecular rotations, which concerns gases

and some liquids, are studied in the far infrared region.

This section presents experimental infrared methods which will

enable one to determine information about the interface that is formed when

an oxide is grown on a semiconductor. The interface region presents special

problems not evident in the study of other substances by infrared because

of the extremely small thickness of material involved. For this reason

conventional once-pass techniques probably will not be effective. There-fore some type of multireflectance technique is necessary. Studies have been made on thin films using a beam that is reflected between two parallel mirrors. This appears not to be a satisfactory method. The spectrum obtained is a combination of that of the oxide, the semiconductor, and the interface. The effects of the interface will be masked behind those larger effects of the materials. The method recommended is that of <u>Internal Reflections</u>, which will only involve the effects of the semiconductor and the interface, and thus will be easier to discern.

Infrared spectroscopy has traditionally been applied to the study of gases and organic liquids. The information available about these substances is much more extensive than that of solids. Gas molecules are free to rotate and they produce rotational spectra in the infrared region. From this spectra can be obtained the moment of inertia of the molecules, and thus the structure can be deduced quite easily. Solids are not free to rotate, but are usually held in a crystal lattice. Because of these differences, the techniques involved in the study of gases and solids are quite different.

Straightforward boundary value solutions to Maxwell's Equations describe the reflection, transmission and adsorption of electromagnetic radiation. From such an analysis the laws of reflection, refraction, adsorption, and internal reflection are derived.

Associated with the total internal reflection is a penetration depth of the radiation into the lower dielectric constant material at the interface from which the reflection occurs. The material within that penetration depth layer influences the totally reflected beam.

N. J. Harrick studied the phenomenon of total reflection for

applying it to the study of the spectra of surfaces of optically transparent
materials, particuarly semiconductors. Radiation penetrates the surfaces
into the rarer medium to a depth predicted by theory. This radiation is
sensitive to molecular adsorption on the surface. The degree of interac-
tion on each reflection is well comparable with that observed for a single
transmission if the film thickness is equal to or less than the penetration
depth. Since many total internal reflections can be used without power
loss, this technique should be a sensitive one in the study of the chem-
istry of surfaces of optically transparent materials and of thin films
which can be deposited on optically more dense and transparent dielectrics.

Thin samples have been spectrally analyzed by placing them on
polished metal surfaces and, to gain sensitivity, multiply reflecting
the infrared beam between two such mirrors. Even though the reflec-
tivity of the metal may be high, the beam is rapidly attenuated for many
reflections which may be required to gain sensitivity, as the power in
the beam is finally R^n where R is the reflectivity and n is the number of
reflections.

It is particularly important to apply similar techniques to the
study of semiconductor surfaces in order to correlate the chemistry of
the surface with our present knowledge of the physics of the surface.
Powdering the semiconductor has the disadvantage that the characteristics
of the semiconductor may change drastically. A beam transmitted through
a sample consisting of several separated layers has the disadvantage that
reflectivity losses are high. The same disadvantage applies to a greater
degree to a beam multiply-reflected between two parallel plates. Total
internal reflection of radiation above the lattice adsorption edge might
work, because on reflection the beam actually penetrates the surface and

is pumped into and out of the rarer medium. This beam, if it is sensitive to molecular resonances, should give information regarding the type of impurity on the surface and the nature of the bonding to the surface.

Harrick used the total internal reflection technique to study the germanium-air interface. The sample was prepared similar to Fig. 33. Also tested were polyethylene deposits on germanium. It was found that the reflection signal was independent of film thickness except for films less than 0.16 micron thick. This thickness is thus a measure of the depth of the penetration of the radiation in the polyethylene, which falls on the experimental curve. From these results Harrick estimates that through the use of more reflections and a more sensitive spectrometer, one to ten molecular layers can be detected using this technique. This conclusion is reached from the observation that an absorption band in a film 3.0 micron thick was readily detected through the use of only eight reflections and a rather insensitive spectrometer.

Harrick warns of possible difficulties in using this technique. The index of refraction may change rapidly in the vicinity of molecular resonances if the damping effects are small. When this is the case, the condition of total reflection at the interface may no longer be met, and the radiation can then escape the light pipe. It would return to the light pipe if total reflection occurs at the outside boundary of the film on the light pipe and if the radiation is not absorbed completely by the film. Also, in analyzing the spectrum on the surface it is necessary to take into account any absorptions in the bulk: e.g., oxygen in silicon, and the spectrum of the free carriers, e.g., holes. The density of free carriers can be kept at a low value by using either wide band gap or near intrinsic semiconductors and by working at low temperatures if necessary.
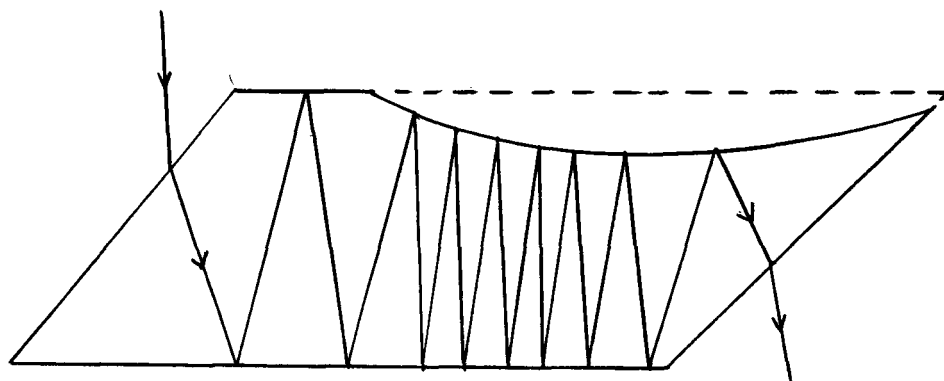
Figure 33
Internal Reflection Specimen Cross Section

In an excellent paper presented in the Journal of Research, E. R. Lippincott and others outline a study they made of the polymorphous forms of silicon-dioxide and germanium-dioxide. Several other investigators have presented a detailed analysis of the vibrational spectrum of quartz. The infrared spectra of cristobalite and fused silica have been reported but no specific assignments of their spectra have been given. Infrared spectra are available for the SiO_2 polymorphs of coesite, cristobalite, tridymite, and vitreous silica; also, the GeO_2 in the region of 4,000 cm^{-1} to 300 cm^{-1} are available. Lippincott gives a partial interpretation of the spectra in terms of respective structures and selection rules. Particular emphasis is placed on locating characteristic frequencies and satisfying the observed frequencies in terms of species of vibrations.

The form of SiO_2 and GeO_2 are basically tetrahedral in nature.
The differences of the polymorphs rely mostly upon how the structure is
coordinated, or how many tetrahedral structures make up the unit cell,
and how they are oriented. A SiO_2 group in a rigid framework has 3N-3
or six vibrational degrees of freedom. The classification of vibrations
in terms of bond stretching, bending, and bond-distortion types are
somewhat arbitrary. Generally, a bond-stretching and bond-bending mode
will be associated with each O atom. These O-stretching modes should
correspond to the highest observed frequencies in the spectrum. Two
remaining degrees of freedom are assigned to the Si atom. One of these
must be a stretching mode corresponding approximately to motions of the
Si atom between the two O atoms. The one remaining mode must correspond
to a low-frequency distortion or bending motion of the Si atom.

Each SiO_2 group which is added to the first to make up the unit
cell adds nine vibrational degrees of freedom. These nine modes may be
classified approximately into the following types. Because each added
SiO_2 group corresponds to the addition of four bonds, four of the nine
modes correspond to bond-stretching frequencies, two involving displace-
ments associated with the O atoms and two for the Si atom. Stated another
way, these correspond to two antisymmetric stretching modes of the type
$\leftarrow$ Si O $\rightarrow$ $\leftarrow$ Si, and two symmetric stretching modes of the type
$\leftarrow$ Si O Si $\rightarrow$. Two more of these nine modes may be classified as bend-
ing motions associated with the bending of the Si-O-Si angle. The remain-
ing three modes are associated with low-frequency bending or distortion
frequencies.

Considerable data and nomenclature are available for the various

crystalline forms of silicon oxide. Extension of the data into glassy

forms will be relatively easy experimentally. The detailed understand-

ing and theoretical development will be more difficult. This technique

appears well worth further study for its applicability to the silicon/

silicon oxide system.

D. Fluorescence of Silicon Oxide

The energy levels of electrons in silicon oxide can be studied by using the luminescent spectrum as well as the absorption spectrum. The various forms of luminescence can go far in revealing the electronic states in the energy band of dielectric materials. This phenomenon appears particularly useful in analyzing the thin film of oxide on single crystal silicon. This oxide has received considerable attention and insufficient clarification.

Numerous references indicate that fluorescence should be observed from most silicon oxide glasses. Characteristic spectra are associated with specific impurities in the glass and process steps in manufacturing the glass. Such behavior has been observed on wet nitrogen oxidized slices of 300 ohm-cm N-type silicon. Figure 34 presents the essential components of a spectrophotofluorometer.

Source   Specimen   Detector

Grating   Grating

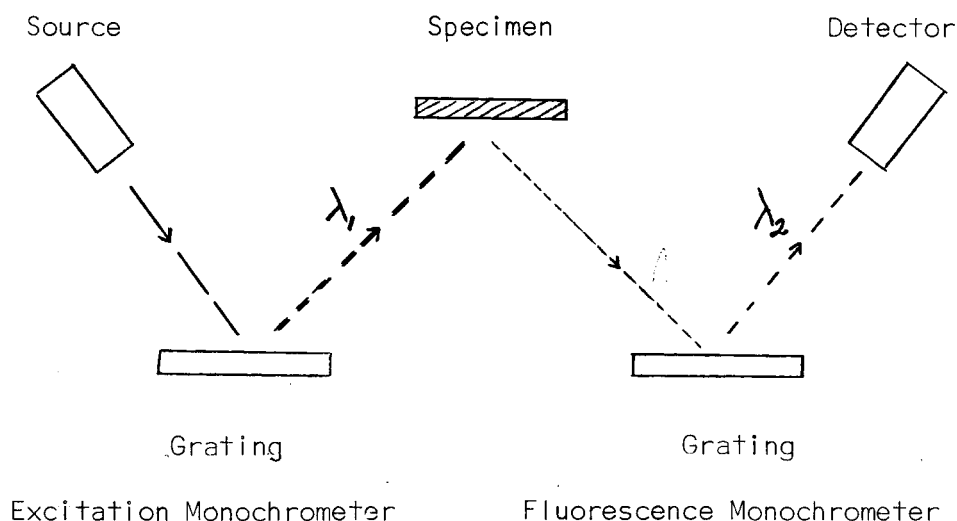Excitation Monochrometer   Fluorescence Monochrometer

Figure 34
Spectrophotofluorometer Components

Specimens of NaCl and fused quartz were observed to fluoresce in the grating spectrophotofluorometer used in this experiment to demonstrate the functioning of the instrument. Boiling sulfuric acid removed any organic materials on the surface which could give misleading fluorescence. Figure 35 presents the quantity of fluorescence observed in comparison to the background when the slice was washed in hydrofluoric acid to remove the oxide.
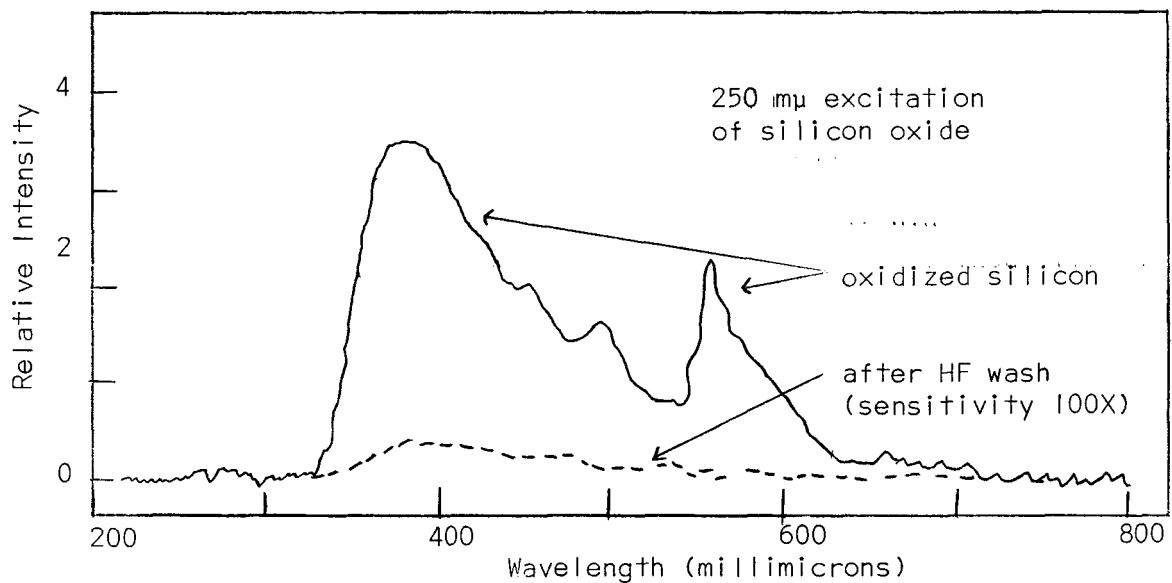
Figure 35
Fluorescence of Oxidized Silicon

The fluorescence intensity from the oxide was approximately 1000 times that of the background after the oxide was removed.

Figures 36, 37, and 38 represent the detailed curves for the fluorescent spectrum of three specimens when illuminated with 300 mμ radiation. The three specimens are (a) oxidized 300 ohm-cm N-type silica, (b) oxidized silicon with B_2O_3 present, and (c) oxidized silicon with P_2O_5 present.

Figure 36
Fluorescence Spectrum of an Oxidized Silicon Crystal

Figure 37

Fluorescence Spectrum of Boron-Doped Oxide

Figure 38
Fluorescence Spectrum of Phosphorus-Doped Oxide

Scattered first and second harmonics of the grating produce the large peaks

at 300 and 600 $m\mu$. Improved instrumentation will eliminate those peaks
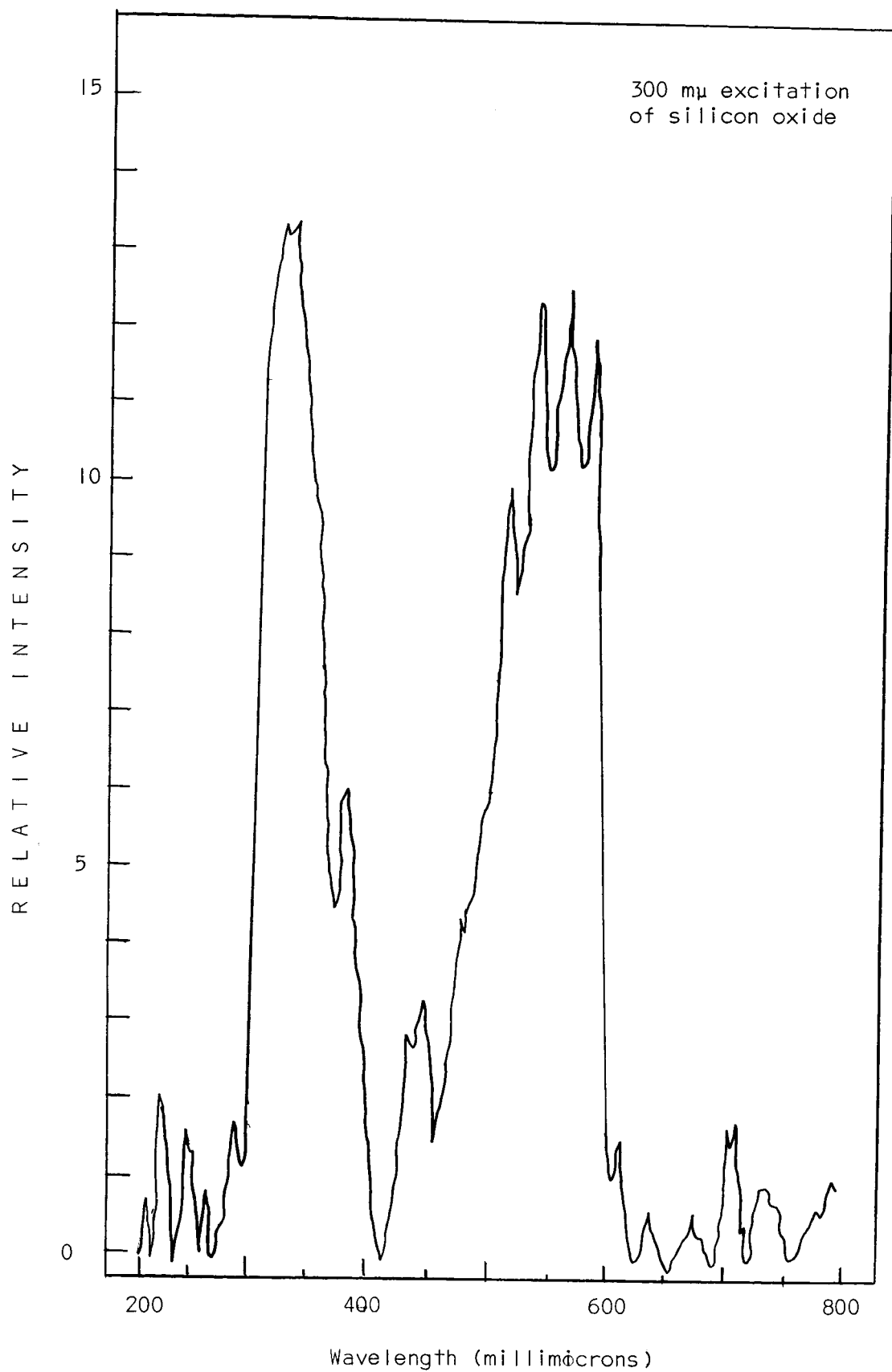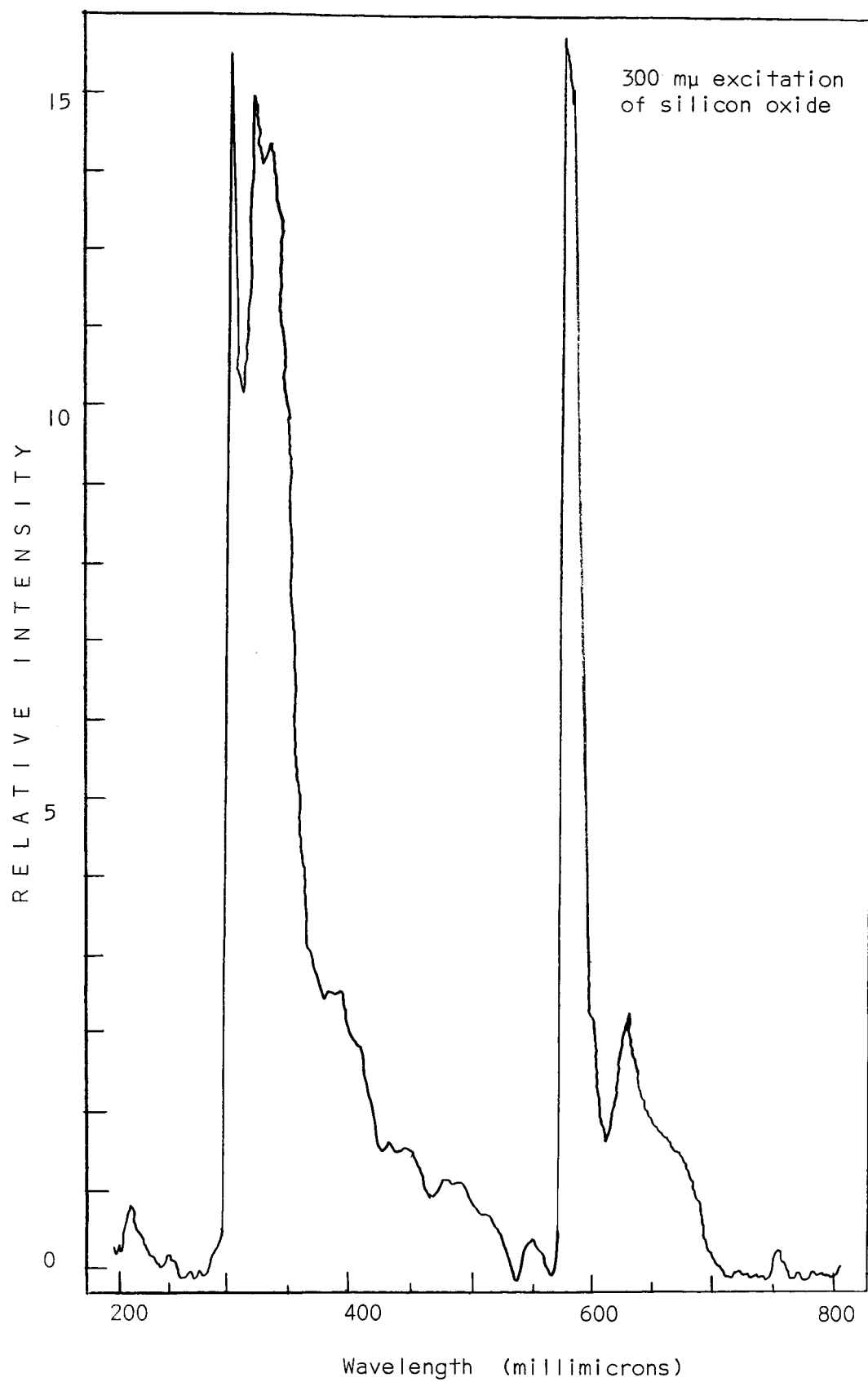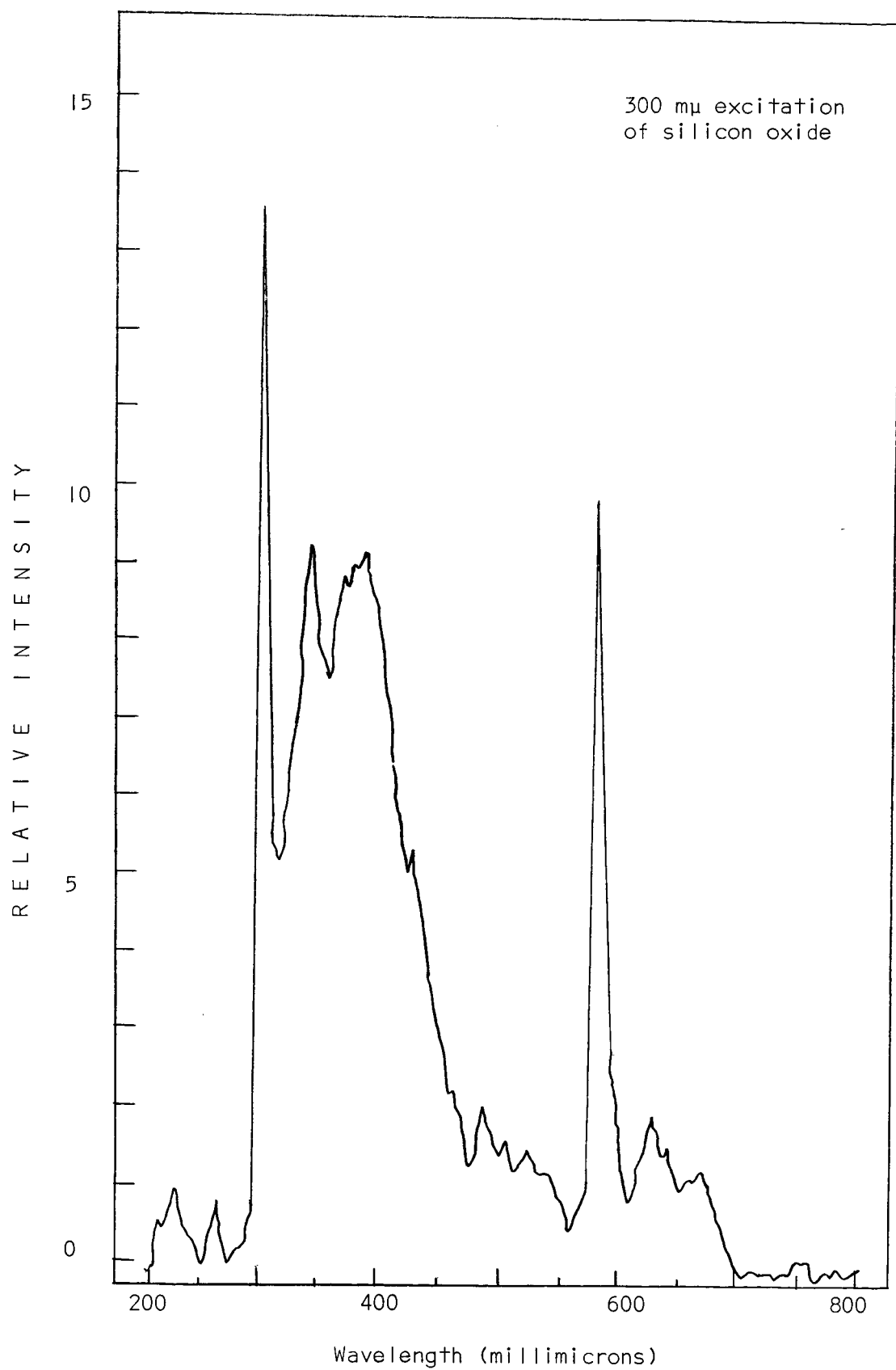
to produce a better analysis of the fluorescence.

The opportunity of identifying specific impurities in the oxide

by fluorescence is apparent. All the specimens produced fluorescence

at a number of wavelengths from 215$m\mu$ to 750$m\mu$. The oxide on the rela-

tively pure crystal produces lines not observed in either of the doped

oxides. Boron produces a number of lines not seen from the others, expec-

ially from 280-345$m\mu$ and 655 - 675$m\mu$. The phosphorous-doped oxide gave

the least characteristic spectra. The most notable fact at this time is

the comparatively little fluorescence from the phosphorous-doped oxide.

The few lines in it not exhibited by the others appear to be slight

displacements of a line appearing in the boron-doped oxide. Figure 39

presents on a linear scale an approximate simplified spectrum for the

four cases: (1) all specimens, (2) only pure oxide, (3) only boron-doped,

and (4) only phosphorous-doped oxide. These wavelengths were chosen from
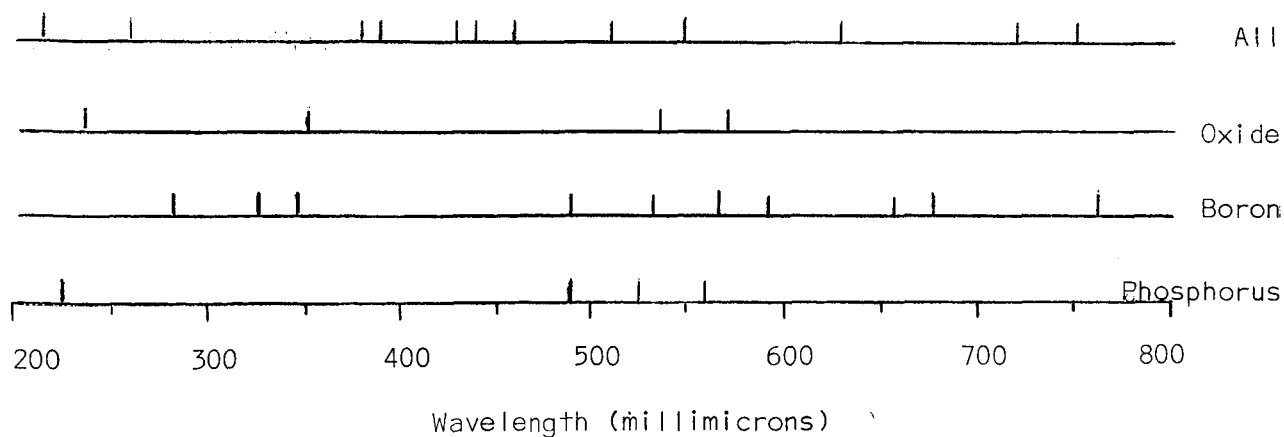
Figure 39
Reduced Fluorescence Spectra

a graphical correlation of observations of excitation from five different excitation wavelengths.

This work indicates a tremendous promise for increasing the understanding of the detailed electronic state and structural defect centers in thin films of materials as are now commonly used in microelectronics. Fluorescence has long been an analytic tool of the mineralogist and the organic chemist. Solid state electronic materials can be profitably analyzed by fluorescence also. The only spectral line which appears to correspond with absorption spectra published by Kats and Stevels is the 550 mµ line which could be attributed to aluminum or iron impurity or structural defects.

The observed spectra are too complex to analyze in terms of defect centers without considerable additional data. Multiple excitation wavelengths and multiple specimen temperatures of observation can make possible analysis in terms.of the configuration coordinate curve model.

VI. Potential Quality Control Measurements

While executing this research program, possible ways for utilizing the results in improved device manufacture are also considered. At this time many of these possibilities could be established in proper form for prompt utilization.

Beginning slices of silicon can be examined for crystallographic orientation by x-ray diffraction. Evaluation of the size and shape of Laue back-reflection patterns can grossly determine if considerable strain or dislocations are in the material. Highly perfect crystals can be examined by the anomalous transmission observed in thick specimens of near perfect crystals. X-ray techniques could also evaluate the strain and dislocations induced by diffusion steps in the process.

Visible light ellipsometry can check the uniformity of surface condition on the cleaned and polished specimens prior to oxidation. Phase contrast and polarized light optical microscopy could also be used but with less sensitivity. Gross strains in the slice could be measured by ellipsometry at a wavelength transmitted by the material.

Surface smoothness of the slice can be measured by interferometry, grazing incidence optical scattering, optical microscopy, or electron microscopy depending on the dimensional variation to be measured. The electrical and composition surface properties can be observed by fluorescence of the silicon, the fluorescence of the oxide film on the silicon, the secondary electron emission from the surface, or the electron mirror properties of the surface.

Spot checks on the ion bombardment needed for producing an atomically clean surface in ultra-high vacuum could be another indication of the surface

film remaining after chemical cleaning. Significant metallic impurities remaining on the surface could be observed by low-energy electron diffraction.

The properties and uniformity of the oxide can be evaluated by most of the optical and electronic techniques previously mentioned. Optical techniques offer a wide range of contactless, non-contaminating measurements. Luminescence offers an untried technique for qualitative and quantitative analysis of surface properties and homogeneity of oxides, photolithographic coatings, photolithographic residues, and diffusion impurities in the oxide.

Once electrical contacts have been attached to the slice, conductivity, current-voltage characteristics, transient measurements, and noise measurements can be made in much the same manner as is partially used at this time. Photo-stimulation can be combined with most of the electrical measurements. The kind of measurements to be made obviously will vary according to the device. Special structures such as M-O-S capacitors, diodes, and photoconductive strips can be incorporated into the wafer mask layout to make available on each slice all the kinds of structures considered informative about the process.

Use of all the mentioned techniques on any one device process is unlikely. The value of some can be readily evaluated as small for a particular process and given no further consideration. Each general kind of process should be studied in detail to determine which measurement capability can give the needed information easily and inexpensively. Enough measurement techniques are available that such process analysis should enable the process engineer to revise the process to improve significantly the long term reliability as well as the uniformity of the product.

BIBLIOGRAPHY

1. R. J. Archer,
   "Determination of the Properties of Film on Silicon by the Method
   of Ellipsometry, Bell Telephone Co.,
   Journal of the Optical Society of America, Sept. 1962, pp 970-77

2. Bell Laboratories Record ,
   "New Technique for Nearly Perfect Laser Mirrors,
   pages 412-414, January, 1965

3. R. C. Benson and Mr. R. Mirarchi,
   "The Spinning Reflector Technique for Ruby Laser Pulse Control",
   IEEE Transactions on Military Electronics , pp 13-31   January, 1964

4. F. A. Brand, H. Jacobs, S. Weitz, and J. Strozyk,
   "Optical Maser Detection by Microwave Absorption in the Semiconductors",
   IEEE International Convention Record, Part 3, pp 162-166, 1963

5. Brown and Twiss,
   Proceedings of the Royal Society of London, Vol. 242, p. 300, 1957

6. V. J. Cocoran and Y. H. Pao,
   "Detection of Laser Radiation ",
   Optical Society of America Journal, Vol. 52, pp 1341-1350, December
   1962

7. B. E. Deah, and A. S. Grove, E. H. Snow, and C. L. Sah,
   "Observation of Impurity Redistribution During Thermal Oxidation of
   Silicon Using the M-O-S Structure,"
   Journal of the Electrochemical Society, Vol. 112, No. 3, (March 1965)

8. S. Deb, P. K. Chowdhury, and M. K. Mukherjee,
   Journal of Scientific and Industrial Research, Vol. 22, p 326,
   August, 1963

9. R. W. Ditchburn
   "Some New Formulas for Determining the Optical Constants from Measure-
   ment of Reflected Light,
   J. Optical Society of America, V. 45, pp 743-81, 1955

10. C. Elbaum,
    "On Dislocations Formed by the Collapse of Vacancy Discs",
    Phil. Magazine, Vol 5, pp 669-674, 1960

11. Forrester, Gudmundsen, and Johnson,
    Physical Review, Vol. 99, p 1691, 1955

12. G. C. B. Garrett and W. H. Brattain,
    "Physical Theory of Semiconductor Surfaces,"
    Phys. Rev., Vol 99, No. 2, pp 376-388, July 15, 1955

13. Mino Green,
    "Some Aspects of the Chemistry of Germanium and Silicon Surfaces,"
    Journal of the Physics and Chemistry of Solids, 14, pp 77-86,
    July, 1960

14. A. E. Grove, E. H. Snow, B. E. Deal, and C. L. Sah,
    "Simple Physical Model of the Space Charge Capacitance of Metal-
    Oxide-Semiconductor Structures,"
    J. Appl. Phys, Vol 35, No. 8, pp 2458, August, 1964

15. N. J. Harrick,
    "Surface Chemistry from Spectral Analysis of Totally Internally
    Reflected Radiation,"
    Journal of Physical Chemistry, 64, 1110, 1960

16. R. W. Hellwarth,
    "Control of Fluorescent Pulsations,"
    Advances in Quantum Electronics, edited by J. R. Singer, Columbia
    University Press, New York, pp 334-341, 1961

17. R. W. Hellwarth and F. J. McClung,
    "Giant Optical Pulsations from Ruby,"
    Bulletin of the American Physical Society, Vol. 5, p 414,
    November, 1961

18. J. Horton,
    Dynamics of Solid State Q-Switched Lasers, Masters Thesis, Univer-
    sity of Texas, August, 1964, unpublished,

19. D. R. Kerr, J. S. Logan, P. J. Burkhardt, and W. A. Pitskin,
    "Stabilization of SiO_2 Passivation Layers with P_2O_5",
    IBM J. Res. Dev., Vol 28, No. 4, pp 376-384, September, 1964

20. D. S. Kerr,
    "Effect of Temperature and Bias on Glass-Silicon Interfaces,"
    IBM J. Res. Dev., Vol. 8, No. 4, pp 385-392, September, 1964

21. S. Koozekanani, P. P. Debye, A. Krutchkoff, and M. Ciftan,
    Proceedings of IRE, Vol. 50, p 207, 1962.

22. K. Lehovec, et. al.,
    "Field Effect Capacitance Analysis of Surface States on Silicon",
    Phys. Stat. Sol., Vol 3, pp 447-464, 1963

23. R. Lindner,
    "Semiconductor Surface Varactor,"
    B. S. T. J., Vol XLI, No. 3, May, 1962

24. P. N. Mace and G. McCall,
    "The Effect of Optical Pump Pulse Shape on Ruby Inversion,"
        Proceedings of IEEE, Vol. 53, p 74, January, 1965

25. T. H. Mainman,
    "Stimulated Optical Emission in Fluorescent Solids, I. Theoretical
    Considerations,"
        Physical Review, Vol 123, pp 1145-1151, August 15, 1961

26. F. J. McClung and R. W. Hellwarth,
    "Characteristics of Giant Optical Pulsations from Ruby",
        Proceedings of IEEE, Vol 51, pp 46-53, January, 1963.

27. F. McCracken, et. al.,
    "Measurement of the Refractive Index of Very Thin Films and the
    Optical Properties of Sources by Ellipsometry,
        J. of Research, Sect. A(NBS), V. 67, N. 4, July, 1963, pp 363-77

28. M. Menat,
    "Giant Pulses from a Laser: Optimum Conditions",
        Journal of Applied Physics, Vol. 36, pp 73-76, January 1965

29. Microelectronics Research on Silicon/Silicon Oxide Structures and
    Interfaces ,
        Electronics Materials Research Laboratory, University of Texas,
        Austin, Texas, August 31, 1964

30. Microelectronics Research on Silicon/Silicon Oxide Structures and
    Interfaces",
        Electronic Materials Research Laboratory, University of Texas,
        Austin, Texas, November 30, 1964

31. D. P. Miller, J. E. Moore, and C. R. Moore,
    "Boron Induced Dislocations in Silicon",
        J. Appl. Phys., Vol 33, No. 8, pp 2648-2652, August, 1962

32. F. Partovi,
    "Theoretical Treatment of Ellipsometry,
        J. Optical Society of America, Vol 52, No. 8, pp 918-25

33. R. Plumb,
    "Analysis of Elliptically Polarized Light",
        J. Optical Society of America, Vol 50, No. 9, September, 1960,
        p 892.

34. R. W. Roberts,
    "Generation of Clean Surfaces in High Vacuum",
        British Journal of Applied Physics, 14, September 1963, pp 537-41

35. E. H. Snow, A. S. Grove, B. E. Deal, and C. L. Sah,
    "A Study of Ion Migration in Thin Insulation Films Using the M-O-S
    Structure,"
        presented at the AIME Conference of Electronic Materials, Boston,
        September 21, 1964

36. J. M. Stevels,
     "The Electrical Properties of Glass,"
          Encyclopedia of Physics, Vol. 20, S. Flugge, Editor, Berlin,
          Springer-Verlag, 1957.

37. L. M. Terman,
     "An Investigation of Surface States at a Silicon/Silicon Oxide
     Interface Employing M-O-S Diodes,"
          Dissertation, University Microfilms, Inc., Ann Arbor, Michigan

38. J. E. Thomas, and D. R. Young,
     "Space Charge Model for Surface Potential Shifts in Silicon Passivated
     with Thin Insulation Layers",
          IBM J. Res. Dev. Vol 8, No. 4, pp 368-375, September, 1964

39. U. S. Dept. of Commerce,
     Ellipsometry, Paper PB-121663, March, 1956

40. W. G. Wagner and B. A. Lengyel,
     "Evolution of the Giant Pulse in a Laser",
          Journal of Applied Physics, Vol 34, pp 2040-2046, July, 1963.

41. A. Yariv,
     "Energy and Power Considerations in Injection and Optically Pumped
     Lasers",
          Proceedings of IEEE, Vol 51, pp 1723-31, January, 1963.

42. K. Zaininger,
     Ellipsometry--A Valuable Tool in Surface Research,
          RCA Review, March, 1964, Vol 25, No. 1, pp 85-111.